Reviews in Mineralogy & Geochemistry
Vol. 62, pp. 117-154, 2006

Water in Nominally Anhydrous Crustal Minerals: Speciation, Concentration, and Geologic Significance

Elizabeth A. Johnson*

Department of Earth and Space Sciences
University of California, Los Angeles
Los Angeles, California, 90095, U.S.A.
e-mail: johnsoel@ucla.edu
(*present address: Dept. of Geology & Environmental Sciences, James Madison Univ., Harrisonburg, VA, 22807)

INTRODUCTION

Importance of nominally anhydrous minerals in the crust

Why should we be interested in trace hydrous species in nominally anhydrous minerals in the Earth's crust? After all, hydrous minerals dominate the pedosphere and are abundant to fairly common trace minerals in many metamorphic and igneous crustal rocks. On the other hand, the most abundant minerals in the crust—feldspars, quartz, pyroxenes, and garnet—are all nominally anhydrous. They are present even in systems with low total volatiles or fluid contents, or environments with low water activities where hydrous minerals are unstable. These nominally anhydrous minerals provide an opportunity to expand the extent of our knowledge of fluid composition and water activity, as well as the influence of water on physical properties and geochemical signatures of rocks.

One advantage to investigations of the crustal component of the lithosphere is that many parts of the crust (especially the continental crust) are available for direct study in outcrops at the surface of the Earth. This allows the nominally anhydrous mineral and its hydrous species to be placed into the context of the hand sample, the outcrop, and even the regional geology.

Scope and goals of this chapter

It would be unrealistic to try to cover every water-bearing mineral in the Earth's crust in this chapter. I have limited my discussion to minerals that do not require hydrous species to complete their stoichiometry, and those for which research has been completed on natural crustal samples. These minerals are: quartz, the feldspars, nepheline, pyroxenes, garnets (except pyrope), kyanite, andalusite, sillimanite, rutile, cassiterite, zircon, titanite, cordierite, and beryl. This selection of minerals restricts the discussion primarily to the continental crust below about 3 km depth. Some references to eclogitic and mantle-wedge minerals are included for completeness.

This is a fairly new field of study, and as such, the goal of this chapter is to give an overview of the work that has been done, and more importantly, provide directions for future work. The chapter begins with an overview of the types of hydrous species and the range of absolute concentrations for each mineral or mineral family. The second section provides examples of applications of these measurements to problems of geologic interest.

It is assumed that the reader is familiar with the compositions and general structure and crystal chemistry of these minerals. It is also helpful to have a general understanding of absolute OH concentration measurement techniques, and a reading knowledge of polarized infrared spectra of hydrous species in minerals. Overviews of these topics may be found in

1529-6466/06/0062-0006$05.00 DOI: 10.2138/rmg.2006.62.6

Rossman (1988, 2006); Libowitzky and Beran (2006); Smyth (2006). Hydrogen abundance measurements discussed in this chapter are generally obtained using manometric or infrared spectroscopic methods. A summary of infrared spectroscopic calibrations for common mineral species is given in Table 2 of Rossman (2006). The reader should consult the reference of interest for detailed information about the absorption coefficient used in a particular study.

HYDROUS SPECIES AND CONCENTRATIONS IN CRUSTAL MINERALS

Quartz and coesite

Quartz, a common crustal mineral, contains structural OH groups, macroscopic fluid inclusions, and nanoscale "fluid inclusions" or water clusters (especially seen in synthetic quartz). Previous studies have compiled detailed summaries of the hydrous species in natural and synthetic quartz, chert, opal, and chalcedony (Aines and Rossman 1984a; Rossman 1988).

The infrared spectrum of OH in a natural quartz crystal from Brazil is shown in Figure 1. Diffusion and electrolytic exchange experiments in natural and synthetic α-quartz have established that these sharp bands are due to OH groups associated with other H^+ or monovalent cations including Li^+, Na^+, K^+, Cu^+, and Ag^+, and hydroxyl associated with Al^{3+} (Kats 1962; Aines and Rossman 1984a; Rovetta et al. 1986; Miyoshi et al. 2005). This structural OH is most commonly found in large, clear, undeformed quartz crystals from high-temperature pegmatites as well as synthetic quartz, although some structural OH bands may occur in spectra of other low-temperature forms of quartz (such as amethyst) (Aines and Rossman 1984a; Kronenberg and Wolf 1990). The OH bands in quartz have been calibrated (Chakraborty and Lehmann 1976) and the reported range of OH concentrations is <1 to ~40 ppm H_2O wt. (1-270 H/10^6 Si; Table 1) (Chakraborty and Lehmann 1976; Rovetta et al. 1986; Kronenberg and Wolf 1990; Grant et al. 2003). The structural OH bands broaden and merge together upon heating quartz to just below the α-β transition temperature (586 °C) (Aines and Rossman 1985).

Quartz can also hold up to 8000 ppm H_2O wt. (0.8 wt%) in the form of submicroscopic fluid inclusions (Kronenberg and Wolf 1990). Natural quartz always contains water inclusions that behave as fluid- i.e., they freeze to ice at low temperatures (Kronenberg and Wolf 1990). On the other hand, synthetic quartz contains "clusters" of water molecules that do not transform to ice upon freezing (Aines et al. 1984; Aines and Rossman 1984a; Kronenberg and Wolf 1990; Cordier and Doukhan 1991). Although not strictly structurally incorporated water, these fluid inclusions or water clusters have a large effect on the physical properties of quartz (see discussion below and Appendix for a list of studies).

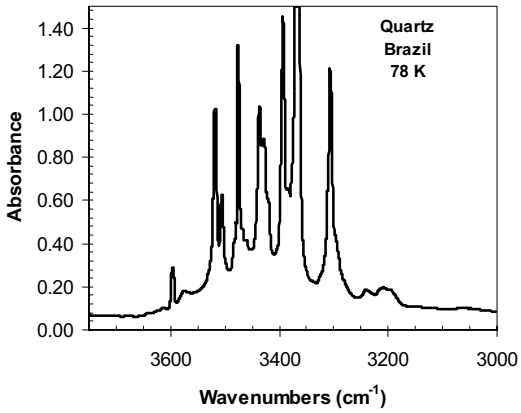

Figure 1. Polarized (**E** perpendicular to *c*) infrared spectrum of OH in a natural Brazilian quartz crystal. Sample is 5 mm thick; spectrum was obtained at 78 K. Data replotted from Aines and Rossman (1984a).

Table 1. OH concentrations in nominally anhydrous crustal minerals.

Mineral	Hydrous species	[OH} range (ppm H_2O wt.)	
		Typical	**Maximum**
Quartz	OH	<1-40	40
	fluid inclusions	0-8000	8000
Coesite	OH	0	135†
Feldspar	OH	0-510	915
	H_2O	135-1350	1350
	NH_4^+	450-1500	buddingtonite
	sub-μm inclusions	0-2300	4265
Nepheline	H_2O	500-3500	5500
Clinopyroxene	OH	<5-240	466
Orthopyroxene	OH	26-117	350
Garnet*	OH	0-4000	14400
Kyanite	OH	<3-44	44
Sillimanite	OH	0-137	200
Andalusite†	OH	270	270
Rutile	OH	310-620	723
Cassiterite	OH	2-120	170
Zircon	crystalline OH	0-100	100
	secondary OH	0-1000	1000
Cordierite	H_2O	3000-24000	24000

*Macroscopic garnets.
† Only one data point available.

Natural coesite found in eclogite assemblages contains no OH within detection limits (Rossman and Smyth 1990; Mosenfelder et al. 2005). The only exception is coesite inclusions in diamond with a reported OH concentration of about 135 ppm H_2O (Koch-Müller et al. 2003).

Feldspars and nepheline

The feldspar group contains the widest range of hydrous species of any mineral group. This, in addition to the structural complexity of the feldspars, creates a diverse array of possible structural incorporation mechanisms in these minerals.

Feldspars may contain structural OH, structural H_2O molecules, ammonium ions (NH_4^+), and submicroscopic fluid inclusions (Hofmeister and Rossman 1985b; Solomon and Rossman 1988; Beran et al. 1992; Johnson and Rossman 2003; Johnson and Rossman 2004). Representative infrared spectra of these hydrous species in feldspars are plotted in Figure 2. Structural OH is characterized by broad (~600 cm^{-1}) absorption bands, with the maximum intensity in the *X* optical direction (Johnson and Rossman 2003). The detailed shape and peak position of the OH bands is roughly a function of composition. Plagioclase feldspars have OH bands centered at 3200-3300 cm^{-1}, whereas alkaline feldspars containing OH have bands at ~3060-3450 cm^{-1} (Johnson and Rossman 2004). Low albite, unlike the other plagioclase feldspars, contains fluid inclusions and very sharp bands assigned to OH, similar to the OH bands for quartz (Wilkins and Sabine 1973; Johnson and Rossman 2003). Beran (1987) proposed that OH substitutes for oxygen on the $O_c m$ site in labradorite.

The alkali feldspars microcline and anorthoclase also contain structural H_2O molecules, and some anorthoclase and possibly sanidine may contain a combination of structural H_2O and OH (Beran 1986; Xia et al. 2000; Johnson and Rossman 2004). There are two types of structural H_2O: one with asymmetric and symmetric stretching frequencies at 3450 and 3630 cm^{-1}

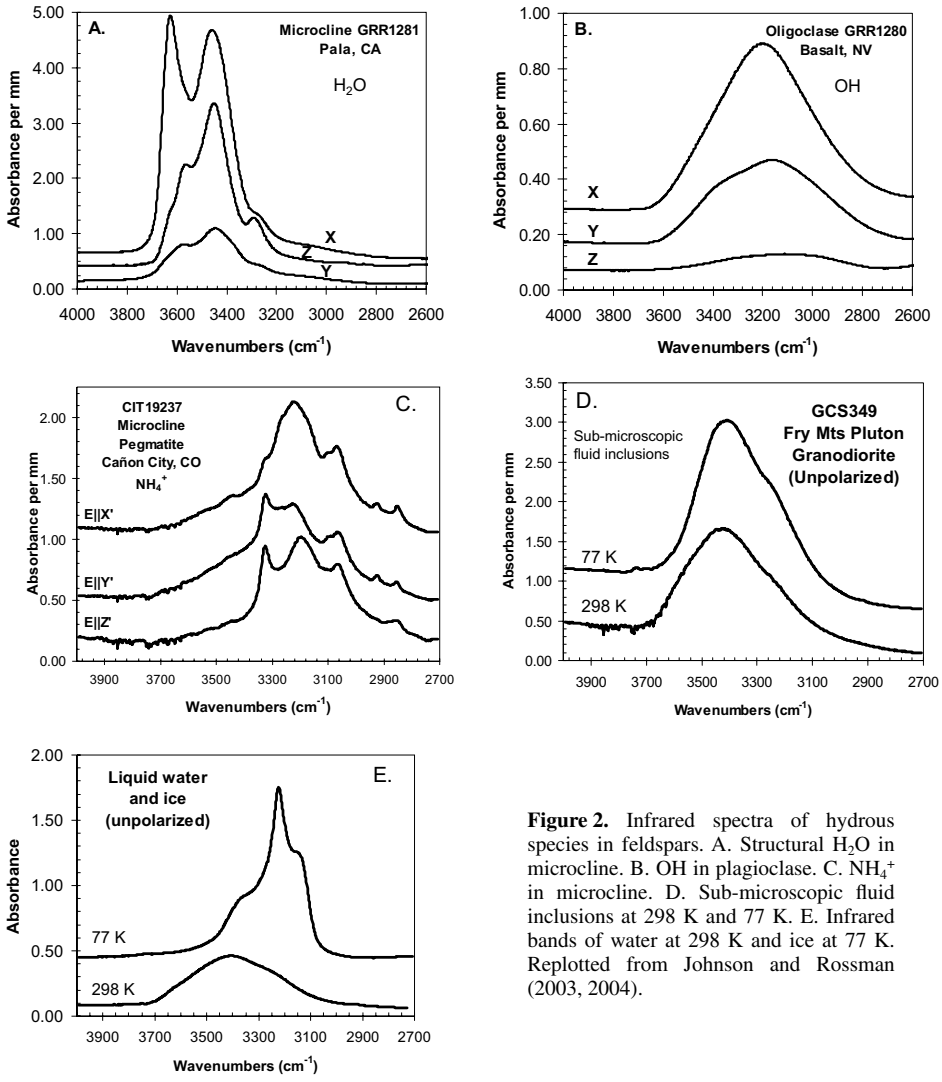

Figure 2. Infrared spectra of hydrous species in feldspars. A. Structural H_2O in microcline. B. OH in plagioclase. C. NH_4^+ in microcline. D. Sub-microscopic fluid inclusions at 298 K and 77 K. E. Infrared bands of water at 298 K and ice at 77 K. Replotted from Johnson and Rossman (2003, 2004).

with absorbance greatest in *X*, and a second type with stretching frequencies at 3285 and 3575 cm^{-1} with maximum absorbance in *Z*. It has been hypothesized that one of these two types of structural H_2O substitutes into the large cation (K^+) site in the structure via a charge-coupled substitution with Ca^{2+}; the second type of H_2O may be associated with the large cation site or with defects in the structure along exsolution lamellae boundaries (Hofmeister and Rossman 1985b; Kronenberg and Wolf 1990). Structurally bound ammonium ions have also been reported in microcline from pegmatites and hyalophane (Solomon and Rossman 1988; Beran et al. 1992).

Finally, plutonic and metamorphic feldspars contain either fluid inclusions that are <1 μm in size, or water "clusters." Unlike microscopic fluid inclusions, these inclusions do not freeze to ice at 77 K (Fig. 2) and may contain alteration products including epidote, clays, and sericite (Johnson and Rossman 2004).

Crystal structure does affect the possible speciation of hydrogen in feldspars (Nakano et al. 2001). Figure 3 shows the infrared spectra of cogenetic albite and microcline from a pegmatite vein. The K-rich lamellae of the microcline contain structural H_2O, the Na-rich lamellae contain fluid inclusions, and the albite crystal contains structural OH and fluid inclusions.

The abundances and species of hydrogen in feldspars are plotted in Figure 4 and listed in the Appendix. All of the hydrous species are present in pegmatite feldspars, but volcanic feldspars contain only structural OH (and melt inclusions). Absolute OH concentrations in volcanic feldspars are not dependent upon major-element composition (Johnson and Rossman 2004). Feldspars from intrusive bodies other than pegmatites contain only sub-micrometer

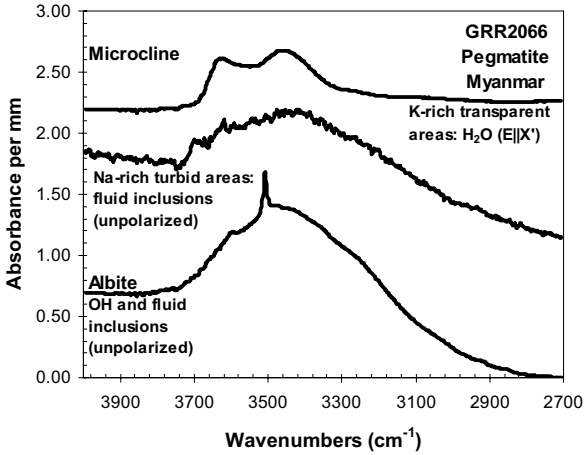

Figure 3. Infrared spectra of hydrous species in coexisting perthitic microcline and albite in a pegmatite. Replotted from Johnson and Rossman (2004).

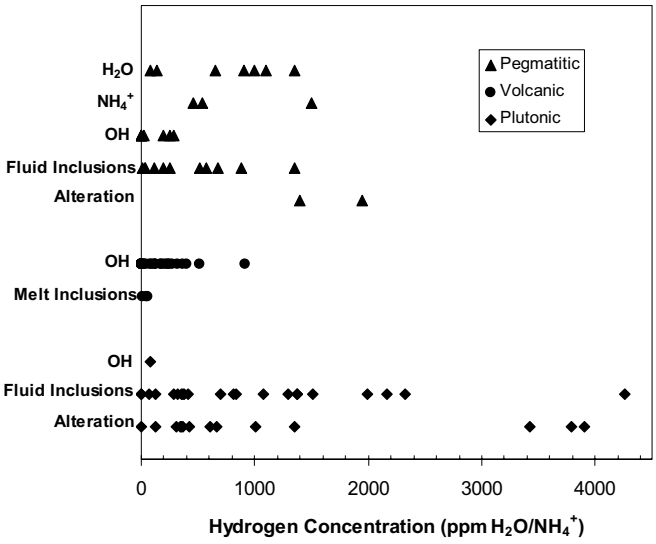

Figure 4. Concentrations of hydrous species in feldspars plotted by rock type. Data from Johnson and Rossman (2004).

fluid inclusions or "water clusters" and secondary alteration minerals. The highest (likely) OH concentration recorded for feldspar is 915 ppm in a volcanic phenocryst (Xia et al. 2000). Structural H_2O concentrations in feldspars range from 80-1350 ppm H_2O (Table 1).

Nepheline, $(Na,K)AlSiO_4$, is a nominally anhydrous feldspathoid mineral that contains structural H_2O molecules (Beran 1974). There are two types of structurally distinct H_2O sites in nepheline, and a third type develops upon heating to 300 °C (Beran and Rossman 1989). All three types of water have their H-H vectors oriented perpendicular to the *c*-axis. Absolute water concentrations in nepheline range from 0.05 to 0.55 wt% H_2O (Beran and Rossman 1989; Balassone and Beran 1995) (Table 1).

Pyroxenes

Pyroxenes contain structural OH groups. An overview of structure of OH in pyroxenes and crystal chemical relationships is given in Skogby (2006) and Smyth (2006). Polarized infrared spectra of OH in diopside and enstatite are shown in Figure 5. Diopside and enstatite typically have four bands in the 3350-3645 cm^{-1} region, whereas omphacite and augite have only one to two distinct OH bands. Amphibole lamellae and disordered pyribole and jimthompsonite

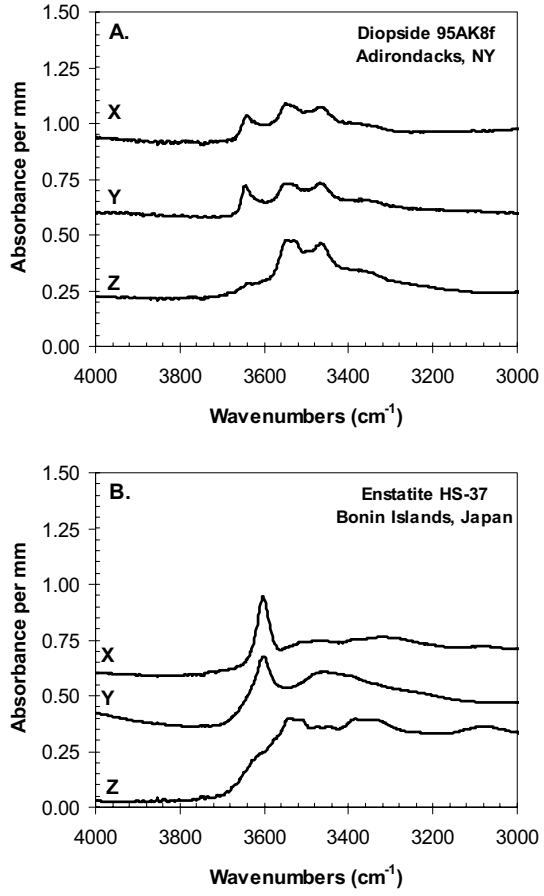

Figure 5. Polarized single-crystal infrared spectra of A) diopside and B) enstatite. Data from Skogby et al. (1990); Johnson et al. (2002).

produce very narrow bands (~10 cm^{-1}) at energies of 3650 cm^{-1} and higher (Skogby et al. 1990). Spodumene spectra have three bands at 3395, 3410, and 3434 cm^{-1}, and some samples have a second set of bands in the 3474-3490 cm^{-1} region (Filip et al. 2006).

Concentrations of OH in natural pyroxenes are plotted in Figure 6 according to general rock type or geologic origin (Skogby et al. 1990; Bell et al. 1995; Johnson et al. 2002; Peslier et al. 2002). In general, clinopyroxenes have higher OH concentrations than orthopyroxenes that formed under similar conditions. Mantle pyroxenes and those from basaltic xenoliths have higher OH concentrations than volcanic phenocrysts and pyroxenes from high-grade metamorphic regimes. Crustal pyroxenes with the highest OH concentrations (up to 466 ppm H_2O) are found in pegmatites and authigenic environments. Table 1 lists the range of OH concentrations for crustal and select mantle samples.

Garnets

Obtaining quantitative analyses of OH in garnets is more straightforward than for many other minerals due to their cubic symmetry. However, the OH band patterns for garnet are some of the most complicated and difficult to interpret. The garnet group includes extensive solid solution between at least seven end-member compositions, including the hydrogrossular ($Ca_3Al_2(OH)_{12}$) end-member and the intermediate hydrated garnets hibschite and katoite. Here I concentrate on the trace to minor OH concentrations in the common crustal garnets with compositions in the grossular-andradite and spessartine-almandine fields. Pyrope is principally a mantle mineral, and is reviewed in Beran and Libowitzky (2006).

The hydrogarnet substitution ($(OH)_4 \leftrightarrow SiO_4$) is an important mechanism for incorporation of water (hydroxyl) into the garnet structure, and the structure of the $(OH)_4$ clusters has been evaluated with neutron diffraction (Bartl 1967; Lager et al. 1987a; Lager et al. 1989). Although an attempt to locate the hydrogen in a low water content garnet using neutron diffraction was not successful (Lager et al. 1987b), a proton nuclear magnetic resonance study of grossular garnets found evidence for clusters of two OH groups as well as the hydrogrossular

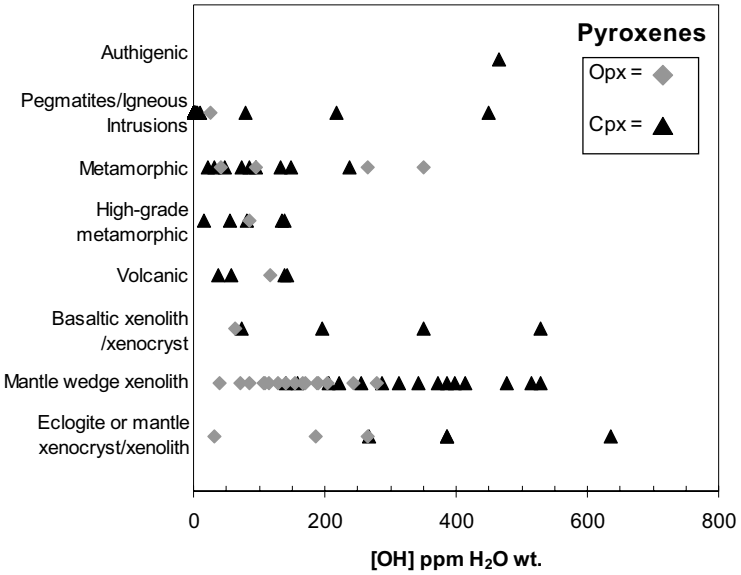

Figure 6. OH concentrations of crustal and mantle pyroxenes plotted according to rock type. Data from Skogby et al. (1990); Bell et al. (1995); Johnson et al. (2002); Peslier et al. (2002).

substitution (Cho and Rossman 1993). The major element composition of garnets has an effect on average OH band position, width, and complexity (Fig. 7), as well as the infrared absorption coefficient used for quantitative analysis (Rossman et al. 1988; Rossman 2006). The origin of the fine structure of the OH bands is not well understood, but may be due to crystal chemical substitutions of cations in sites adjacent to the OH in the structure (Aines and Rossman 1984b; Andrut and Wildner 2001).

Some optically birefringent garnets, especially Ca-rich garnets from hydrothermal or metasomatic deposits, have anisotropic OH bands in the infrared (Rossman and Aines 1986). The origin of this pleochroism is unknown, but may be associated with defects along twinned growth sectors (Allen and Buseck 1988; Hofmeister et al. 1998). A study of birefringent natural uvarovite garnets concluded that $SiO_3(OH)$ tetrahedral groups are an important mechanism of OH defects in garnets with low water contents (Andrut et al 2002).

Figure 8 shows garnet OH concentrations according to geologic provenance (Aines and Rossman 1984b; Rossman and Aines 1991; Locock et al. 1995; Amthauer and Rossman 1998; Arredondo et al. 2001; Johnson 2003). The typical OH concentration in mantle pyrope is much lower than concentrations reported in Aines and Rossman (1984b) (Figure 8; Beran and Libowitzky 2006). The maximum reported OH concentration for natural microscopic hydrogrossular garnets is 20 wt% H_2O (O'Neill et al. 1993), but in most macroscopic garnets concentrations range from below detection limits up to 0.4 wt% (4000 ppm H_2O) (Table 1).

Al_2SiO_5 polymorphs

The Al_2SiO_5 polymorphs (kyanite, sillimanite, and andalusite) are found in a variety of metamorphic crustal and mantle rocks including amphibolites, granulites, and eclogites. Representative polarized infrared spectra of these minerals are plotted in Figures 9, 10, and 11 (Beran et al. 1989; Bell et al. 2004a; Burt et al. 2006). The absorbance bands in these spectra are assigned to structural hydroxyl groups. It can be seen that even though these

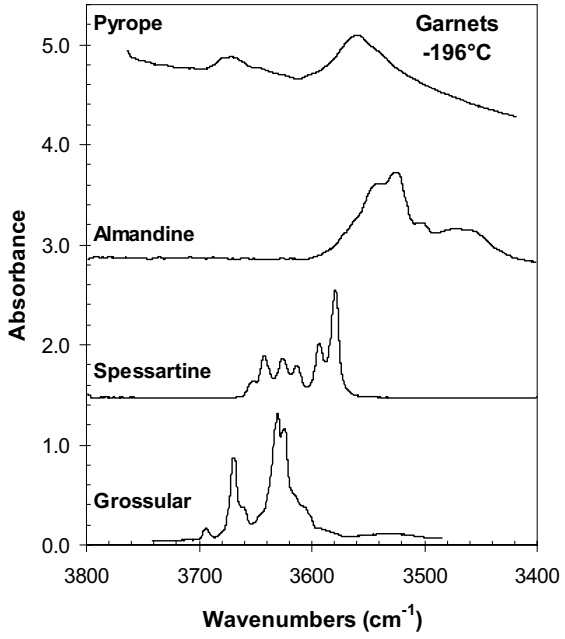

Figure 7. Typical single-crystal infrared spectra of pyrope, almandine, spessartine, and grossular obtained at –196 °C. Data from Aines and Rossman (1984b).

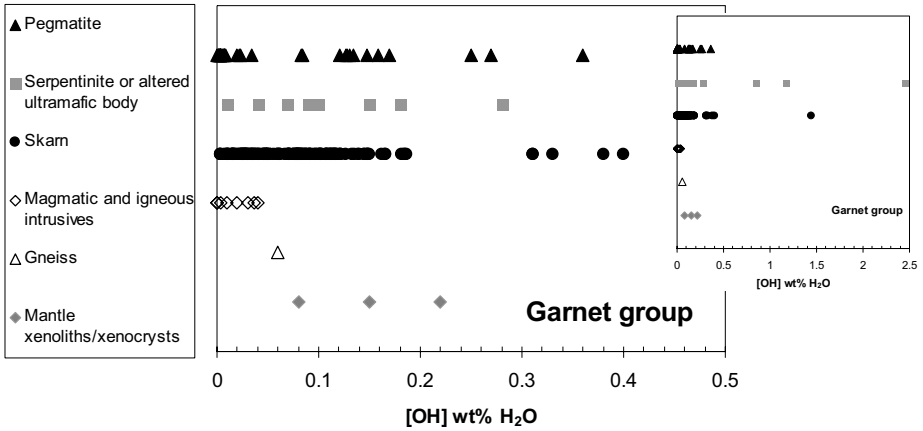

Figure 8. The OH concentration in crustal garnets plotted according to rock type. Representative mantle garnets are also plotted. Data are from Aines and Rossman (1984b); Locock et al. (1995); Amthauer and Rossman (1998); Arredondo et al. (2001); Johnson (2003).

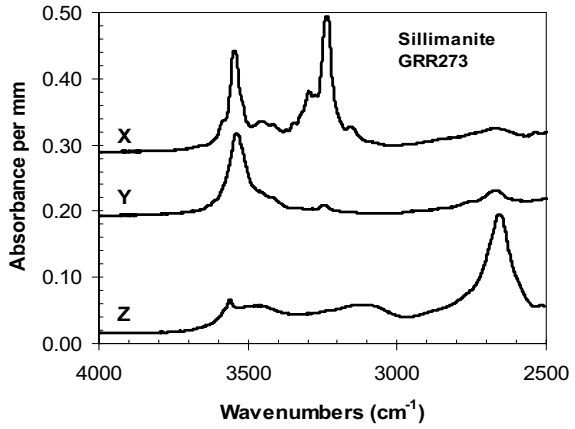

Figure 9. Polarized single-crystal infrared spectra of structural OH bands obtained on sillimanite from Reinbolt Hills, Antarctica (GRR 273). Data replotted from Beran et al. (1989).

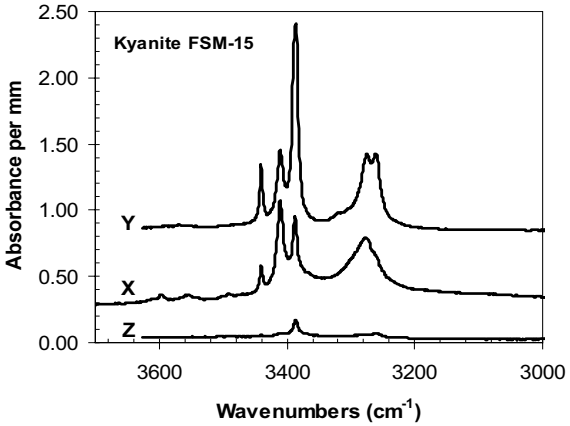

Figure 10. Polarized single-crystal infrared spectra of structural OH bands obtained on kyanite from a kyanite- and corundum-bearing eclogite xenolith from the Frank Smith kimberlite, South Africa. Data replotted from Bell et al. (2004a).

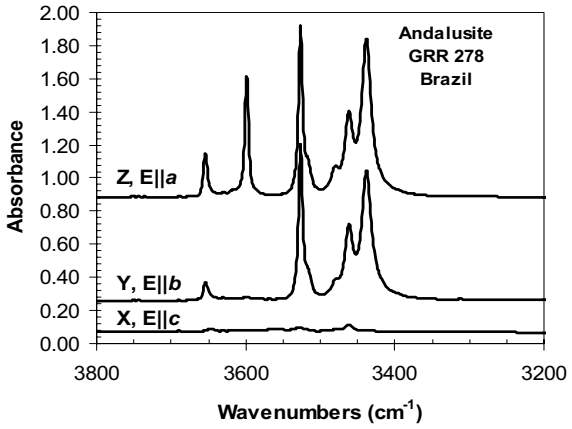

Figure 11. Polarized single-crystal infrared spectra of structural OH bands of andalusite from Minas Gerais, Brazil. Data from Burt et al. (2006).

minerals have identical compositions, their OH band patterns and therefore the local hydrogen bonding environments are different (Libowitzky 1999). The structural OH does not seem to be associated with trace constituents such as Fe or B in sillimanite (Beran et al. 1989). This, together with the limited crystal chemistry of the Al_2SiO_5 polymorphs, suggests that hydrogen is incorporated into these minerals via the exchange mechanism:

$$3(OH)^- + \text{vacancy} \leftrightarrow Al^{3+} + 3O^{2-} \quad (1)$$

The OH concentrations in these minerals should therefore reflect the water activity during peak metamorphism (Beran et al. 1989).

The absolute concentrations of OH in the Al_2SiO_5 polymorphs are low compared to many other nominally anhydrous minerals (Table 1; Appendix). The total range of OH concentrations observed in kyanite (Fig. 12) is 3-230 ppm H_2O, with the highest concentrations in kyanite from eclogite xenoliths (Beran and Götzinger 1987; Beran et al. 1993; Bell et al. 2004a). The maximum OH concentration in kyanite calculated from the calibration of Bell et al. (2004a) is much smaller than previously estimated using conductometry (Beran and Götzinger 1987). The reported range of OH in sillimanite is 0-200 ppm H_2O. Figure 13 shows OH concentration in sillimanite plotted by metamorphic facies, in order of inferred water activity and temperature range. The maximum OH concentration increases with increased expected water activity in the system. Only one OH concentration has been reported for andalusite: a sample from Brazil contains 270 ppm H_2O (Rossman 1996).

One reason there are not more analyses of aluminosilicates may be the difficulty in avoiding abundant fluid inclusions and alteration minerals trapped within cleavage planes. Beran et al. (1989) found that weight loss (assumed to be water) from sillimanite measured over the range 23 °C to 500 °C did not affect the intensities of the structural OH modes in the sample.

Rutile and cassiterite

Polarized infrared spectroscopic studies have determined that hydrogen is incorporated into the rutile (TiO_2) structure as hydroxyl groups and that the OH vector orientation is perpendicular to the *c* crystallographic axis (Rossman and Smyth 1990; Swope et al. 1995). This strong directional anisotropy of OH in the rutile structure results in pronounced absorbance features in spectra obtained with the electric vector (**E**) of incident infrared light perpendicular to *c*, and small or undetectable absorption in the spectrum obtained when **E** is parallel to the *c* crystallographic axis (Fig. 14). There is one prominent OH band present at 3280 cm^{-1} in spectra of both natural and synthetic rutile (Rossman and Smyth 1990; Vlassopoulos et al. 1993;

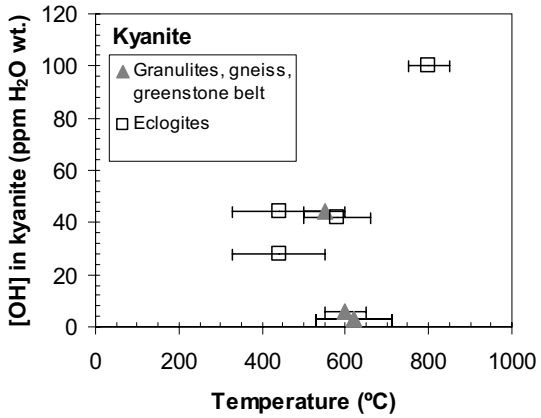

Figure 12. The OH concentration in kyanite as a function of peak metamorphic temperature for crustal rocks and mantle xenoliths. Data are from Beran and Götzinger (1987), and have been recalculated according to the most recent infrared calibration of kyanite (Bell et al. 2004a).

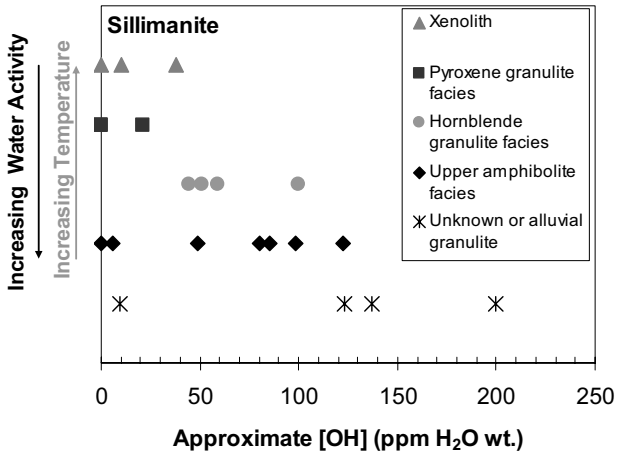

Figure 13. The approximate OH concentration in sillimanite plotted according to rock type and in order of inferred peak metamorphic temperature and water activity. Data are from Beran et al. (1989), with approximate OH concentrations estimated with the calibration given in that study.

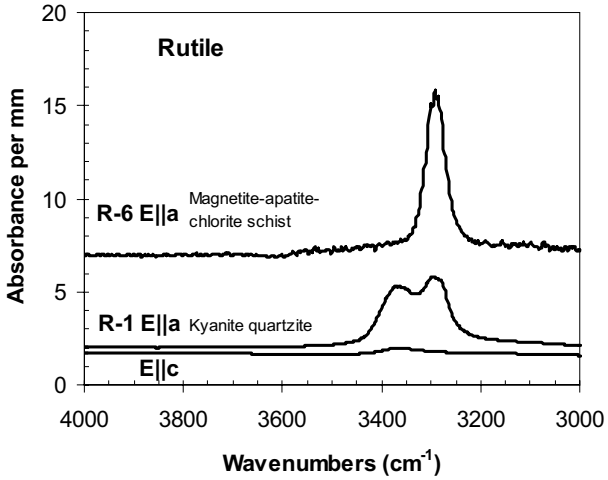

Figure 14. Polarized single-crystal infrared spectra (with the **E**-vector oriented parallel to the *a*- and ***c***-crystallographic axes) of structural OH bands of rutile from a magnetite-apatite-chlorite schist (R-6) and a kyanite quartzite (R-1). Data replotted from Vlassopoulos et al. (1993).

Bromiley et al. 2004). Some infrared spectra of natural samples also have one additional, minor band present at 3320 cm^{-1} or 3360 cm^{-1} (Vlassopoulos et al. 1993). The limited number of OH bands and therefore distinctly different OH sites is presumably related to the fairly simple, high-symmetry structure and limited solid solution chemistry for rutile.

Several previous studies (Rossman and Smyth 1990; Hammer and Beran 1991; Vlassopoulos et al. 1993; Maldener et al. 2001) reported infrared band areas or OH concentrations of natural rutile crystals. The OH concentration data for natural rutile have not been compiled previously in the literature, at least in part because the reported OH concentrations were determined using different values for the integrated absorption coefficient (Johnson et al. 1973; Hammer 1988; Maldener et al. 2001). The OH concentrations from the four studies were recalculated (or calculated) if necessary, using the absorption coefficient from Maldener et al. (2001). These studies report only a general rock type of origin for many of the rutile crystals, allowing the rutile OH concentrations to be categorized very roughly in terms of increasing temperature and pressure (Fig. 15). The maximum OH concentration generally increases with increasing inferred temperature and pressure. Minimum reported OH concentrations are 70-100 ppm H_2O by weight. The maximum OH concentrations are found in mantle samples, up to a maximum of about 2770 ppm (Appendix).

Cassiterite, SnO_2, has a structure identical to that of rutile. The infrared spectra and polarization behavior of OH in cassiterite are therefore not surprisingly very similar to those of rutile; peaks occur at ~3350 cm^{-1} and ~3250 cm^{-1}, with the latter sometimes split into two bands centered on that energy (Losos and Beran 2004). The range of OH concentrations found in natural cassiterite (Appendix) is 32-170 ppm H_2O (Maldener et al. 2001; Losos and Beran 2004).

Zircon and titanite

Zircon, $ZrSiO_4$, is a common accessory mineral in igneous and metamorphic rocks, and is especially useful to geochronologists because trace U and Th incorporated into the structure (and their daughter products) can be used for radiometric dating. Although fluid inclusions and alteration minerals such as clays may contribute bands to the mid-infrared spectra of turbid zircons, most zircons contain only structural OH (Woodhead et al. 1991a). The nature of the structural OH and resulting band pattern in the infrared spectra (Fig. 16) depend upon the degree of metamictization of the crystal (Woodhead et al. 1991a,b). Crystalline zircon contains well-ordered OH that is anisotropic and is manifested by sharp bands in the infrared spectra. As the degree of radiation damage increases, broad, isotropic bands increasingly dominate the spectra. These bands are also assigned to structural OH, because of a lack of absorbance in the water combination mode region (5250 cm^{-1}) (Woodhead et al. 1991a,b). Broader OH bands are indicative of a wider range of OH hydrogen bonding distances (Libowitzky 1999) brought on by structural damage.

The overall concentrations of OH in zircon (Table 1) are not well established, because of a lack of published extinction coefficients for zircon (Bell et al. 2004b). Estimated OH concentrations in zircon are given based on the assumption that the absorption coefficient for OH in zircon is similar to that of grossular garnet (Rossman and Aines 1991). There is limited data available for both crustal and mantle zircons, but the maximum estimated "crystalline" OH concentration, ~0.01 wt% H_2O (100 ppm), was found in a zircon megacryst from a kimberlite (Woodhead et al. 1991a). Maximum "primary" OH concentration is estimated at 0.05 wt% H_2O for a partially metamict zircon from a hydrothermal vug.

The maximum metamict OH concentration (primary or secondary hydration) in zircon is about 0.1 wt% H_2O (Woodhead et al. 1991a). A study of Sri Lankan zircons from alluvial deposits that have undergone various degrees of radiation damage, from very little to a large degree of metamictization, found that the crystalline zircons from this area contain very little to no OH, but the metamict ones have a great deal of the broad-band, isotropic OH (Woodhead

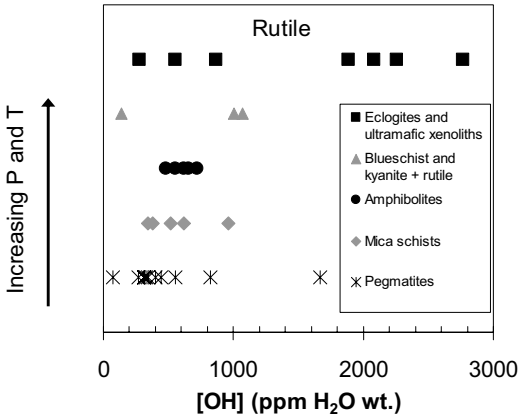

Figure 15. The OH concentration in rutile plotted according to rock type and in order of approximate increasing pressure and temperature. Data are from Rossman and Smyth (1990); Hammer and Beran (1991); Vlassopoulos et al. (1993); Maldener et al. (2001) and are recalculated using the calibration of Maldener et al. (2001).

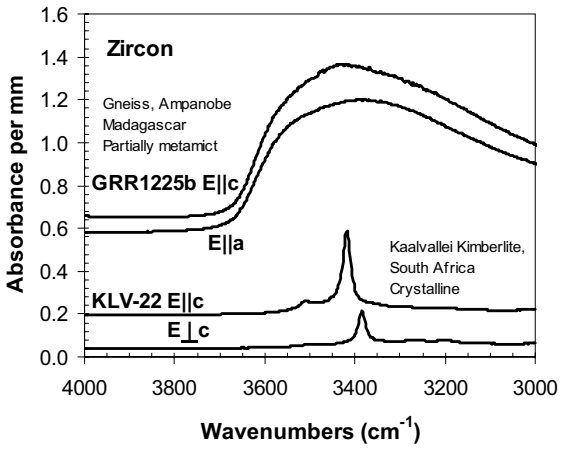

Figure 16. Representative polarized infrared spectra of OH bands obtained on partially metamict (Gneiss, Madagascar) and crystalline (Kaalvallei, South Africa) zircons. Data are from Woodhead et al. (1991a); Bell and Rossman (1992).

et al. 1991b). This shows that this type of broad-band OH is taken up by the mineral after structural damage occurs, and is not an original part of the mineral (Nasdala et al. 2001).

Titanite, $CaTiSiO_5$, also takes up trace U and Th into its structure (Hawthorne et al. 1991), and therefore also suffers radiation damage and metamictization. There is a single crystalline OH band at 3486 cm^{-1}, with maximum absorbance in the *X* direction (Beran 1970). This band broadens, especially on the low energy side <3486 cm^{-1}, with increasing metamictization (Zhang et al. 2001).

Cordierite and beryl

Cordierite, $(Mg,Fe)_2Al_4Si_5O_{18}$ and beryl, $Be_3Al_2Si_6O_{18}$, can incorporate cations and small molecules within the channels running parallel to the *c*-axis of these minerals. A summary of the structure and types of channel water in cordierite and beryl can be found in Rossman (1988). A brief description of the structure of H_2O and CO_2 in cordierite, and a summary of studies that have used volatiles in cordierite to attempt to evaluate metamorphic fluid compositions are provided here.

There are two types of structurally distinct H_2O molecules in cordierite (Fig. 17). Type I H_2O has its H-H vector oriented parallel to the *c*-axis (and channels), while type II H_2O is oriented with its H-H vector perpendicular to the *c*-axis (Farrell and Newnham 1967; Aines

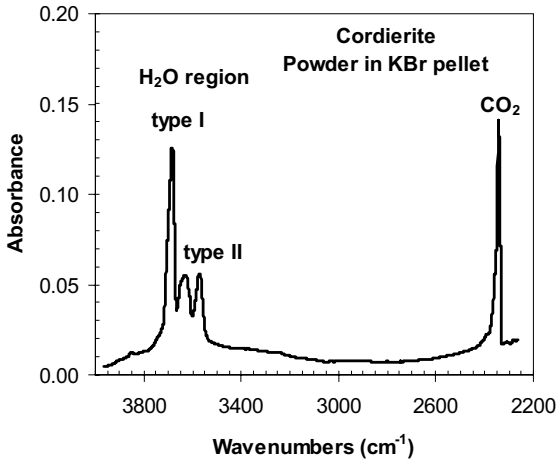

Figure 17. Unpolarized infrared spectrum of a KBr pellet of powdered cordierite. Bands are assigned to type I and II H_2O and CO_2 in the channels within the cordierite structure. Data from Vry et al. (1990).

and Rossman 1984c; Rossman 1988; Kolesov and Geiger 2000). Type II H_2O is associated with large cations such as Na, K, and Ca that are also incorporated into the channels. Many natural cordierites also contain CO_2 in their channels, with the molecular axis oriented parallel to the *a*-axis (Aines and Rossman 1984c; Kolesov and Geiger 2000). At high temperatures, both type I and II water are dynamically disordered, and dehydration of water occurs by 800 °C; loss of CO_2 is complete by 900 °C (Aines and Rossman 1984c). Two studies have reported hydrocarbons in cordierite (Mottana et al. 1983; Khomenko and Langer 1999).

End-member Mg cordierite can theoretically hold up to 2.99 wt% H_2O or 6.99 wt% CO_2 (Vry et al. 1990). Typical concentrations of H_2O in cordierite range from 0.3 to 2.04 wt% and CO_2 concentrations range from 0.1 to 2.2 wt% (Armbruster et al. 1982; Vry et al. 1990; Swamy et al. 1992; Visser et al. 1994; Kalt 2000). Although it may seem to be the perfect monitor of fluid composition, crystal chemistry (particularly cations in the channels) and grain size can bias uptake of water over CO_2 during metamorphism (Vry et al. 1990). Post-metamorphic re-equilibration may also affect the resulting estimated water activity of the system (Visser et al. 1994). A complete list of studies involving cordierite as an indicator of metamorphic fluid history is given in the Appendix.

UNDERSTANDING GEOLOGIC SYSTEMS

As shown above, structural hydrous species are incorporated into essentially all major nominally anhydrous crustal minerals. These studies have established the range of hydrous species concentrations in various crustal minerals as well as the crystallographic orientations of these species. The plots in the previous section of water concentration as a function of general geologic provenance or rock type hint at the type of information that could be derived from these measurements.

This section provides a summary of geologic issues that could be informed by such hydrogen concentration measurements. These issues can be divided into two categories: evaluation of thermodynamic properties of a system, and evaluation of the effect of water on physical properties of common crustal minerals.

Thermodynamic properties

Water concentrations in nominally anhydrous minerals can be used as indicators of water activity or the oxygen fugacity of the geologic environment. This is analogous to using

water contents and Fe^{3+}/Fe^{2+} ratios in hydrous minerals to evaluate water activity and oxygen fugacity (e.g., Lamb and Valley 1988; King et al. 2000). With the exception of cordierite, most minerals hydrous or nominally anhydrous do not incorporate measurable CO_2 into their structures. This means that we can derive the water activity of the system, but not the complete fluid composition or total fluid pressure, without knowing the pressure and temperature of the system. This method of evaluating fluids in the geologic environment is therefore best used where the fluid is predominantly H_2O, or in environments where water is the particular fluid phase of interest. Details of the solubility of water in nominally anhydrous minerals are given in Keppler and Bolfan-Casanova (2006).

The studies described below qualitatively and quantitatively investigate water activity and oxygen fugacity in natural systems using nominally anhydrous minerals.

Garnets as indicators of fluid evolution. Conductive heat loss models indicate that pegmatite veins should crystallize from the outer walls of the vein (wall zone) inwards to the center (core). This progressively concentrates incompatible elements and water in the remaining melt, so that the largest and most beautiful minerals crystallize in the core area of the vein (Lumpkin 1998). Arredondo et al. (2001) measured the OH concentrations of spessartine in transects across three pegmatite bodies (the Rutherford No.2 pegmatite, VA, and the Himalaya and George Ashley Block pegmatites in CA) to establish if pegmatite garnets record the evolution of fluids in these systems. The OH concentrations and the major (Mn) and minor (Fe, Ca) element compositions of the spessartine record a general increase in water content of the melt from wall to core zone for the Rutherford No.2 (Fig. 18) and Himalaya pegmatites, and record a magma reinjection event in the George Ashley Block pegmatite (Arredondo et al. 2001).

Johnson (2003) investigated the zonation of OH and minor elements in cm-sized grossular-andradite garnets from an irregular epidote-grossular-calcite skarn. This skarn is less than 10 meters wide, and formed in a contact metamorphic zone between lower Cambrian sedimentary rocks and the granitic intrusives of the Inyo batholith, located at the foot of Birch Creek on the northwest side of Deep Springs Valley, Inyo County, California (Nash 1962; Shieh and Taylor 1969). In all three of the large, optically zoned garnets investigated, the OH concentration monotonically decreases from core (0.43-0.47 wt% H_2O) to rim (0.14-0.20 wt% H_2O). Although Fe exhibits oscillatory zonation, the Ti concentration in the zoned garnets is highly correlated with the OH concentration, and H and Ti may participate in charge-coupled substitution into the garnet crystal structure. This association of H and Ti in grossular from Birch Creek is not

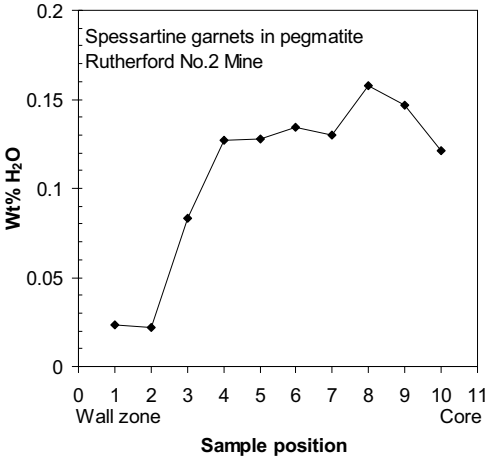

Figure 18. The OH concentration in spessartine garnets from the Rutherford No.2 Pegmatite plotted from the outer wall zone to the center (core) of the pegmatite. Figure modified from Arredondo et al. (2001).

observed in other grossular samples (Rossman and Aines 1991). The small skarn at Birch Creek likely formed during infiltration of magmatic fluid from the late-stage intrusive dike into the surrounding country rock. The solubility of Ti in the fluid phase is expected to decrease sharply with decreasing temperature (Van Baalen 1993). After initial infiltration of magmatic fluid into the carbonate sediments, the system cooled and Ti solubility in the fluid quickly dropped, resulting in the observed OH and Ti zonation in the Birch Creek garnets.

These two studies show that OH concentration measurements can be used to qualitatively investigate the fluid history of igneous and metamorphic rocks.

Volatile composition of melts. The OH concentrations in volcanic phenocrysts could be used to quantitatively evaluate magmatic water content in volcanic systems if the partitioning behavior of hydrogen between nominally anhydrous minerals and melts is known. A few studies have experimentally (Aubaud et al. 2005) and empirically (Dobson et al. 1995; Johnson 2005; Seaman et al. 2006) determined partition coefficients for hydrogen in such systems. The experimental study found the following partition coefficients (D) between coexisting peridotite minerals and a basaltic melt: $D^{(ol/melt)} = 0.0017$, $D^{(opx/melt)} = 0.019$, and $D^{(cpx/melt)} = 0.023$. These D values are not affected by changes in pressure or total water content over the experimental range (1-3 GPa; melt water contents of 3.1-8.8 wt% H_2O). An empirical study (Dobson et al. 1995) determined the partition coefficient of water between orthopyroxene phenocrysts and coexisting boninite glass from the Bonin Islands, Japan, to be 0.003-0.004. Johnson (2005) used hydroxyl concentrations of feldspar phenocrysts and water concentrations of their melt inclusions from the 1980-1981 series of eruptions of Mount St. Helens to come up with D of 0.004. On the other hand, Seaman et al. (2006) recently estimated a partition coefficient for water of 0.1 between anorthoclase crystals and melt inclusions from Mount Erebus, Antarctica. Further work should be done to determine partition coefficient values so that OH measurements may be used to study volatile histories in volcanoes.

Diffusion of hydrous species in minerals plays a potentially important role in preservation of OH abundances in phenocrysts during and immediately after an eruption, especially those that undergo oxidation-dehydration reactions. For example, Fe-bearing minerals such as amphiboles, micas, pyroxenes, and olivine are known to lose structural hydrogen when Fe is oxidized (e.g. Addison et al. 1962; Vedder and Wilkins 1969; Skogby and Rossman 1989):

$$Fe^{2+} + OH^-_{(structure)} = Fe^{3+} + \tfrac{1}{2}H_{2\,(g)} + O^{2-}_{(structure)} \quad (2)$$

Diffusion of hydrogen in minerals is generally several orders of magnitude faster than diffusion of larger cations and oxygen, and is especially rapid when controlled by redox reactions such as Equation (2) (Ingrin and Blanchard 2006). In general, the time elapsed during eruption of a single block of pumice or lava flow is short compared to the time scale of significant diffusive loss of hydrogen from a phenocryst (Johnson 2005), but magma and coexisting phenocrysts may be transported and stored within the Earth before eruption. If transport and storage takes place over time scales longer than hours to weeks, the OH concentration in the nominally anhydrous phenocryst has time to re-equilibrate with the surrounding volatile conditions. It is therefore likely that OH in phenocrysts record volatile contents from the last storage event.

Hydrothermal alteration. The sub-micrometer fluid inclusion concentrations in a suite of feldspars from the epizonal Fry Mountains Pluton, CA, were determined in Johnson and Rossman (2004). These samples represent varying degrees of hydrothermal exchange between meteoric water and the granite during cooling (Solomon and Taylor 1991). The concentration of sub-micrometer fluid inclusions in these feldspars generally increases with decreasing $\delta^{18}O$ of the whole rock, a measure of the degree of hydrothermal exchange (Fig. 19). The sub-micrometer fluid inclusions appear to form during the process of oxygen isotope exchange between the feldspar and the meteoric fluids (O'Neil and Taylor 1967; Yund and Anderson 1978; David and Walker 1990; David et al. 1995), and their concentrations could be used as a proxy for the amount of water that has interacted with a given volume of rock in a hydrothermal system.

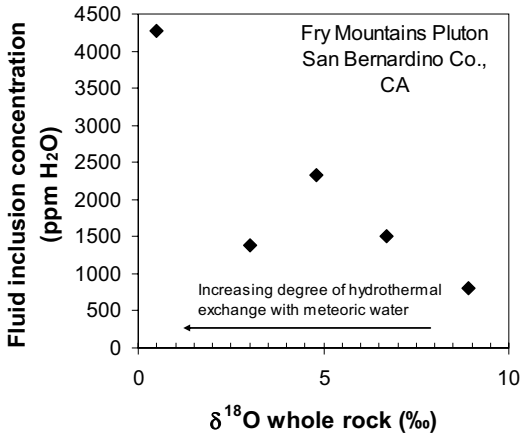

Figure 19. Sub-micrometer fluid inclusion concentration versus whole rock $\delta^{18}O$ for feldspars from the Fry Mountain Pluton, CA. Data from Johnson and Rossman (2004).

Water activity and oxidation state in the lower crust. The fluid conditions in granulite-facies calc-silicate rocks from the Adirondacks Mountains, NY, were investigated by Johnson et al. (2002). The concentration of structural OH in diopside was determined for four different localities in the region for which water fugacities (~0.15-0.8 kbar) had been previously estimated using oxygen isotope systematics (Edwards and Valley 1998). The total diopside OH content ranges from 55 to 138 ppm H_2O by weight, and the OH concentration in diopside increases monotonically with increasing water fugacity (Fig. 20) and linearly with the OH concentrations assigned to bands that increase in intensity during hydrothermal exchange experiments (Skogby and Rossman 1989). There is no significant variation in OH content within a single diopside grain or among diopside grains from the same hand sample. Charge-coupled substitution with M^{3+} and Ti^{4+} in the crystal structure may have allowed retention of OH in the diopside structure during and after peak metamorphism (~750 ºC, 7-8 kbar). The Cascade Slide diopside has an Fe^{3+}/Fe^{2+} ratio of 0.98, compared to 0-0.05 for the other samples, implying that some loss of hydrogen through oxidation of Fe (via Eqn. 2) was possible in this sample. This study shows that OH concentrations in nominally anhydrous minerals containing Fe can be indicators of

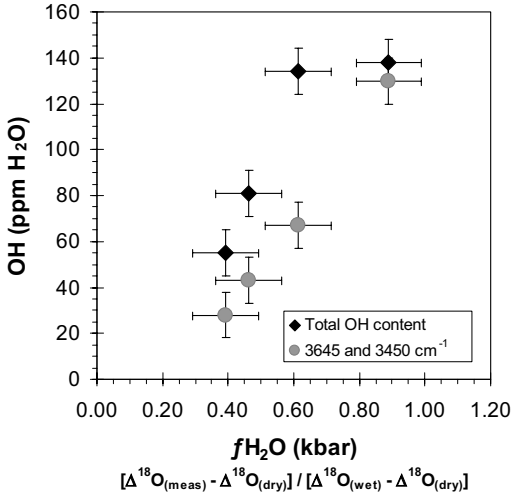

Figure 20. Total OH concentration of diopside (diamonds) and "hydrothermal" OH (circles) plotted versus water fugacity, as predicted from oxygen isotope measurements (Edwards and Valley 1998). Figure modified from Johnson et al. (2002).

water fugacity in the crust for well-characterized rocks, although the redox chemistry of Fe in the crystal structure may interfere with this signal.

Oxidation state of the mantle wedge. Although the Peslier et al. (2002) study of pyroxenes from mantle wedge xenoliths does not deal directly with crustal rocks, it is informative to crustal studies in terms of the relationship it finds between partial melting, oxidation state, and OH concentration in Fe-bearing nominally anhydrous minerals. This study investigated the OH concentrations of orthopyroxene and clinopyroxene from spinel peridotite xenoliths from Mexico and the northwest United States. The OH concentrations of the pyroxenes are correlated with whole-rock Al_2O_3 content, implying that mantle geochemical signatures are preserved in these samples. The ratio of OH concentrations in coexisting clinopyroxene and orthopyroxene is consistently ~2 to 1, and absolute OH concentrations range from 140-528 ppm H_2O in clinopyroxene and 39-265 ppm H_2O in orthopyroxene.

The OH concentrations in the pyroxenes are negatively correlated with calculated oxidation state of the peridotite, expressed as deviations above and below the fayalite-magnetite-quartz (FMQ) oxidation buffer (Fig. 21). This decrease in OH concentration with increased oxidation is thought to be caused by metasomatism of the sub-arc mantle wedge peridotites by oxidized fluids or melts derived from the subducting slab (Peslier et al. 2002). Increased oxidation state drives the redox reaction (2) and dehydration of the pyroxenes.

This process of oxidation by melt or fluid infiltration could also affect the retention of OH in Fe-bearing crustal minerals. It is also interesting to note that the OH concentration in Fe- or Ti-bearing minerals may also be used as an indicator of oxygen fugacity, if the geologic system is well characterized (Johnson et al. 2005).

Physical properties

Water affects the physical properties of minerals and rocks, including deformation rates and shear strength, phase transitions, stabilization of radiation damage, and diffusion rates of major elements such as Al, Si, and O which can in turn affect exsolution processes and geochemical signatures.

Hydrolytic weakening and deformation rates. An overview of the influence of water on rock deformation is given in Kohlstedt (2006). Many experimental studies have examined the influence water has on lowering the temperature of the brittle-ductile transition of quartz (Griggs 1967; Tullis and Yund 1980; Kekulawala et al. 1981; Kronenberg et al. 1986; Ord and Hobbs 1986; Rovetta et al. 1986; Cordier et al. 1988; Gerretsen et al. 1989; Kronenberg and Wolf 1990; Kronenberg 1994; Post and Tullis 1998). The structural OH in natural quartz has a negligible effect on deformation behavior; instead, it is the fluid inclusions that play a major role in structural weakening (Kekulawala et al. 1981; Kronenberg et al. 1986; Gerretsen et al. 1989; Post and Tullis 1998).

Several studies have investigated fluid inclusions in natural quartz samples to better understand the role of fluid inclusions in deformation and hydrothermal alteration of quartz-bearing rocks (Kronenberg and Wolf 1990; Berzina et al. 1991; Nakano et al. 2001; Ito and Nakashima 2002; Niimi 2002). A study of the sheared quartz near the Moine thrust zone in Scotland (Kronenberg and Wolf 1990) reported a general increase in fluid inclusion content of quartz from 4200 ppm H_2O at 110 m from the contact to 7400 ppm H_2O within several centimeters of the contact, although there were large variations in water content among grains from a single hand sample. Another study (Nakashima et al. 1995) of a mylonite zone adjacent to the Median Tectonic Line (MTL) in Japan found that quartz fluid inclusion concentrations increased from 300 ppm H_2O at 800 m from the MTL to 2500 ppm H_2O 100 m away from the MTL (Fig. 22). This study also found a decrease in the fluid inclusion concentration of metacherts with increasing metamorphic grade (Nakashima et al. 1995).

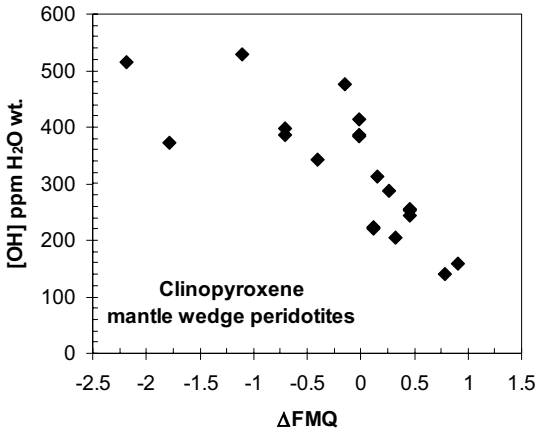

Figure 21. OH concentrations of clinopyroxene from mantle wedge peridotite xenoliths plotted as a function of calculated oxygen fugacity. Data replotted from Peslier et al. (2002).

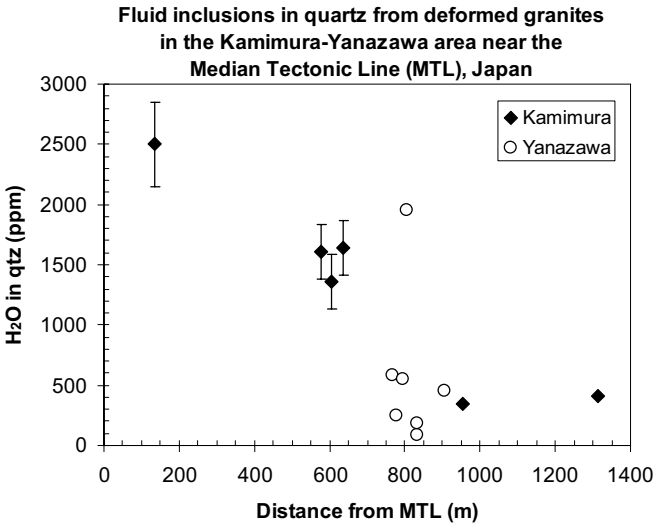

Figure 22. Fluid inclusion H_2O concentrations of quartz from deformed granitic rocks versus distance from the Median Tectonic Line (MTL) mylonite zone. Data replotted from Nakashima et al. (1995).

Phase transformations and radiation damage. There is evidence that hydrous species may promote or stabilize physical transformations in the crystal structure of a nominally anhydrous mineral. For example, coesite in ultrahigh-pressure rocks is preferentially preserved in areas with little or late, low-temperature infiltration of retrograde fluids (Mosenfelder et al. 2005). Experiments have determined that the transformation rate of coesite to quartz is more than an order of magnitude higher for coesite containing structural OH than for "dry" coesite (Lathe et al. 2005).

As discussed previously, "anisotropic" OH in partially or completely metamict zircon and titanite is associated with radiation damage (Hawthorne et al. 1991; Woodhead et al. 1991a,b). This secondary OH likely stabilizes the metamict state (Hofmeister and Rossman 1985b; Aines and Rossman 1986). In some minerals including brown topaz, blue plagioclase, and amazonite, hydrous species help to charge-balance the structure and are key to stabilization

of radiation-damage associated color centers (Aines and Rossman 1986; Hofmeister and Rossman 1986). On the other hand, water molecules inhibit coloration in amethyst and smoky sanidine (Hofmeister and Rossman 1985a; Aines and Rossman 1986).

Diffusion rates of Al, Si, and O. The presence of water dramatically increases the Al-Si interdiffusion rate (Goldsmith 1986, 1987, 1988) as well as the oxygen diffusion rate in many silicate and oxide minerals (e.g., Yund 1983; Farver and Yund 1990; Farver and Yund 1991; Farver 1994). Faster oxygen diffusion rates lower the effective mineral closure temperature and affect the oxygen isotope systematics used to constrain the thermal histories of igneous and metamorphic rocks.

The increased rate of Al and Si interdiffusion in feldspars under hydrous conditions may lead to larger exsolution lamellae and a coarser perthitic texture in alkali feldspars (Yund and Ackermand 1979). It has been suggested that the structural hydrous species such as OH play a role in the Al-Si interdiffusion process in feldspars (Goldsmith 1986; Goldsmith 1988). A comparison of perthitic feldspars from pegmatites showed that those with larger exsolution lamellae have higher hydrogen concentrations (as structural hydrous species and fluid inclusions) than those with smaller exsolution lamellae (Johnson and Rossman 2004).

The water budget of the Earth

Structural hydrous species in nominally anhydrous crustal minerals do not significantly contribute to the overall water budget of the Earth, but sub-micrometer-sized fluid inclusions in feldspars and fluid inclusions in quartz are significant due to their high abundances and the ubiquity of feldspars and quartz in the continental crust. The total mass of water in feldspar inclusions in the upper continental crust is estimated to be about 1×10^{19} kg, assuming that the crust contains 30% feldspar and an average feldspar fluid inclusion concentration of 2000 ppm H_2O (Johnson and Rossman 2004). If quartz (~15% of the upper crust) (McLennan and Taylor 1999) is included in the calculation, again assuming an average fluid inclusion content of 2000 ppm H_2O, the total mass of water residing in nominally anhydrous minerals in the upper crust is $\sim 2 \times 10^{19}$ kg. This is roughly equivalent to the amount of water stored in the hydrous minerals in the upper crust (6×10^{19} kg), and a few percent of the $\sim 4 \times 10^{20}$ kg of water estimated to be stored in nominally anhydrous minerals within the upper mantle (Ingrin and Skogby 2000).

SUMMARY AND FUTURE POSSIBILITIES

The hydrous species in quartz, feldspars, pyroxenes, garnets, kyanite, andalusite, sillimanite, rutile, cassiterite, zircon, titanite, and cordierite include hydroxyl (OH), structural water (H_2O), the ammonium ion (NH_4^+), and sub-micrometer fluid inclusions. Cordierite also commonly includes CO_2 in its channels. Plotting concentrations of hydrous species for a given mineral by rock type or metamorphic grade reveals trends broadly related to the expected water activities for each rock type. The concentrations of these species in each mineral can also be affected by crystal chemistry or structure.

Most of the work involving nominally anhydrous crustal minerals to date has been exploratory. It consists primarily of detailed crystallographic studies of a few mineral samples and surveys of hydrous species and concentrations from exceptional mineral samples from various known and unknown geologic provenances. The handful of studies that have used nominally anhydrous minerals to investigate water activity, oxygen fugacity, and deformation behavior in specific locations or geologic provenances have had encouraging results. This chapter provides guidelines for future studies in this area of research.

ACKNOWLEDGMENTS

The author would like to thank Anton Beran, Eugen Libowitzky, Henrik Skogby, and an anonymous reviewer for careful and constructive criticism that improved this chapter. Jason Burt, Satoru Nakashima, and Julie Vry graciously provided data for figures. I greatly appreciate Hans Keppler's editorial guidance and efforts in organizing this project. Special thanks go to George Rossman, for providing access to old data files, digitizing software, and the Caltech spectroscopic facilities. This work was supported by NSF grant EAR-0409883.

REFERENCES

Addison CC, Addison WE, Neal GH, Sharp JH (1962) Amphiboles: Part I. The oxidation of crocidolite. J Chem Soc 1962:1468-1471

Aines RD, Kirby SH, Rossman GR (1984) Hydrogen speciation in synthetic quartz. Phys Chem Minerals 11: 204-212

Aines RD, Rossman GR (1984a) Water in minerals? A peak in the infrared. J Geophys Res 89:4059-4071

Aines RD, Rossman GR (1984b) The hydrous component in garnets: pyralspites. Am Mineral 69:1116-1126

Aines RD, Rossman GR (1984c) The high temperature behavior of water and carbon dioxide in cordierite and beryl. Am Mineral 69:319-327

Aines RD, Rossman GR (1985) The high temperature behavior of trace hydrous components in silicate minerals. Am Mineral 70:1169-1179

Aines RD, Rossman GR (1986) Relationships between radiation damage and trace water in zircon, quartz, and topaz. Am Mineral 71:1186-1193

Allen FM, Buseck PR (1988) XRD, FTIR, and TEM studies of optically anisotropic grossular garnets. Am Mineral 73:568-584

Amthauer G, Rossman GR (1998) The hydrous component in andradite garnet. Am Mineral 83:835-840

Andrut M, Wildner M (2001) The crystal chemistry of birefringent natural uvarovites. Part I. Optical investigations and UV-VIS-IR absorption spectroscopy. Am Mineral 86:1219-1230

Andrut M, Wildner M, Beran A (2002) The crystal chemistry of birefringent natural uvarovites. Part IV. OH defect incorporation mechanisms in non-cubic garnets derived from polarized IR spectroscopy. Eur J Mineral 14:1019-1026

Armbruster T, Schreyer W, Hoefs J (1982) Very high CO_2 cordierite from Norwegian Lapland: Mineralogy, petrology and carbon isotopes. Contrib Mineral Petrol 81:262-267

Arredondo EH, Rossman GR, Lumpkin GR (2001) Hydrogen in spessartine-almandine garnets as a tracer of granitic pegmatite evolution. Am Mineral 86:485-490

Aubaud C, Withers AC, Hirschmann MM, Guan Y, Leshin LA, Mackwell SJ, Bell DR (2005) A new calibration of H measurements by SIMS in glasses and nominally anhydrous minerals: application to experimental determinations of H partitioning. Eos Trans AGU 86(52), Fall Meet. Suppl. Abstract V41A-1419

Balassone G, Beran A (1995) Variable water content of nepheline from Somma-Vesuvio, Italy. Mineral Petrol 52:75-83

Bartl H (1967) Röntgen-Einkristalluntersuchungen an $3CaO{\cdot}Al_2O_3$ und an $12CaO{\cdot}7Al_2O_3{\cdot}H_2O$; neuer Vorschlag zur $12CaO{\cdot}7Al_2O_3$-Struktur. N Jb Mineral Mh 2-3:33-42

Bell DR, Ihinger PD, Rossman GR (1995) Quantitative analysis of trace OH in garnet and pyroxenes. Am Mineral 80:465-474

Bell DR, Rossman GR (1992) Water in Earth's mantle; the role of nominally anhydrous minerals. Science 255: 1391-1397

Bell DR, Rossman GR, Maldener J, Endisch D, Rauch F (2004a) Hydroxide in kyanite: A quantitative determination of the absolute amount and calibration of the IR spectrum. Am Mineral 89:998-1003

Bell DR, Rossman GR, Moore RO (2004b) Abundance and partitioning of OH in a high-pressure magmatic system: Megacrysts from the Monastery Kimberlite, South Africa. J Petrol 45:1539-1564

Beran A (1970) Messung des Ultrarot-Pleochroismus von Mineralen. IX. Der Pleochroismus der OH-Streckfrequenz in Titanit. Tscherm Mineral Petr Mitt 14:1-5

Beran A (1974) UR-spektroskopischer Nachweis von H_2O in Nephelin. Tschermaks Mineralogische und Petrographische Mitteilungen 21:299-304

Beran A (1986) A model of water allocation in alkali feldspar, derived from infrared-spectroscopic investigations. Phys Chem Minerals 13:306-310

Beran A (1987) OH^- groups in nominally anhydrous framework structures: an infrared spectroscopic investigation of danburite and labradorite. Phys Chem Minerals 14:441-445

Beran A, Armstrong JT, Rossman GR (1992) Infrared and electron microprobe analysis of ammonium ions in hyalophane feldspar. Eur J Mineral 4:847-850

Beran A, Götzinger MA (1987) The quantitative IR spectroscopic determination of structural OH groups in kyanites. Mineral Petrol 36:41-49
Beran A, Langer K, Andrut M (1993) Single crystal infrared spectra in the range of OH fundamentals of paragenetic garnet, omphacite and kyanite in an eklogitic mantle xenolith. Mineral Petrol 48:257-268
Beran A, Libowitzky E (2006) Water in natural mantle minerals II: olivine, garnet and accessory minerals. Rev Mineral Geochem 62:169-191
Beran A, Rossman GR (1989) The water content of nepheline. Mineral Petrol 40:235-240
Beran A, Rossman GR, Grew ES (1989) The hydrous component of sillimanite. Am Mineral 74:812-817
Berzina AP, Sotnikov VI, Kovaleva LT, Gimon VO (1991) Water in quartz of Cu-Mo deposits. Soviet Geol Geophys 32:103-109
Bromiley G, Hilairet N, McCammon C (2004) Solubility of hydrogen and ferric iron in rutile and TiO_2(II): implications for phase assemblages during ultrahigh-pressure metamorphism and for the stability of silica polymorphs in the lower mantle. Geophys Res Lett 31:doi:10.1029/2004GL019430
Burt JB, Ross NL, Gibbs GB, Rossman GR, Rosso KM (2006) Potential protonation sites in Al_2SiO_5 polymorphs based on polarized FTIR spectroscopy and properties of the electron density distribution. (in prep)
Chakraborty D, Lehmann G (1976) Distribution of OH in synthetic and natural quartz crystals. J Solid State Chem 17:305-311
Cho H, Rossman GR (1993) Single-crystal NMR studies of low-concentration hydrous species in minerals: Grossular garnet. Am Mineral 78:1149-1164
Cordier P, Boulogne B, Doukhan JC (1988) Water precipitation and diffusion in wet quartz and wet berlinite $AlPO_4$. Bull Minéral 111:113-137
Cordier P, Doukhan JC (1991) Water speciation in quartz: a near infrared study. Am Mineral 76:361-369
David F, Walker L (1990) Ion microprobe study of intragrain micropermeability in alkali feldspars. Contrib Mineral Petrol 106:124-128
David F, Walker L, Lee MR, Parsons I (1995) Micropores and micropermeable texture in alkali feldspars: geochemical and geophysical implications. Mineral Mag 59:505-534
Dobson PF, Skogby H, Rossman GR (1995) Water in boninite glass and coexisting orthopyroxene; concentration and partitioning. Contrib Mineral Petrol 118:414-419
Edwards KJ, Valley JW (1998) Oxygen isotope diffusion and zoning in diopside; the importance of water fugacity during cooling. Geochim Cosmochim Acta 62:2265-2277
Farrell EF, Newnham RE (1967) Electronic and vibrational absorption spectra in cordierite. Am Mineral 52: 380-388
Farver JR (1994) Oxygen self-diffusion in calcite: Dependence on temperature and water fugacity. Earth Planet Sci Lett 121:575-587
Farver JR, Yund RA (1990) The effect of hydrogen, oxygen, and water fugacity on oxygen diffusion in alkali feldspar. Geochim Cosmochim Acta 54:2953-2964
Farver JR, Yund RA (1991) Oxygen diffusion in quartz: dependence on temperature and water fugacity. Chem Geol 90:55-70
Filip J, Novák M, Beran A, Zbo□il R (2006) Crystal chemistry and OH defect concentrations in spodumene from different granitic pegmatites. Phys Chem Minerals 32:733-746
Gerretsen J, Paterson MS, McLaren AC (1989) The uptake and solubility of water in quartz at elevated pressure and temperature. Phys Chem Minerals 16:334-342
Goldsmith JR (1986) The role of hydrogen in promoting Al-Si interdiffusion in albite ($NaAlSi_3O_8$) at high pressures. Earth Planet Sci Lett 80:135-138
Goldsmith JR (1987) Al/Si interdiffusion in albite: effect of pressure and the role of hydrogen. Contrib Mineral Petrol 95:311-321
Goldsmith JR (1988) Enhanced Al/Si diffusion in $KAlSi_3O_8$ at high pressures: the effect of hydrogen. J Geol 96:109-124
Grant K, Gleeson SA, Roberts S (2003) The high-temperature behavior of defect hydrogen species in quartz: Implications for hydrogen isotope studies. Am Mineral 88:262-270
Griggs D (1967) Hydrolytic weakening of quartz and other silicates. Geophys J Royal Astron Soc 14:19-31
Hammer VMF (1988) Quantitative IR-spectroscopic determination of structural OH-groups in natural rutiles of various occurrences. Z Kristallogr 185:631
Hammer VMF, Beran A (1991) Variations in the OH concentration of rutiles from different geological environments. Mineral Petrol 45:1-9
Hawthorne FC, Groat LA, Raudsepp M, Ball NA, Kimata M, Spike FD, Gaba R, Halden NM, Lumpkin GR, Ewing RC, Greegor RB, Lytle FW, Ercit TS, Rossman GR, Wicks FJ, Ramik RA, Sherriff BL, Fleet ME, McCammon C (1991) Alpha-decay damage in titanite. Am Mineral 76:370-396
Hofmeister AM, Rossman GR (1985a) A model for the irradiative coloration of smoky feldspar and the inhibiting influence of water. Phys Chem Minerals 12:324-332
Hofmeister AM, Rossman GR (1985b) A spectroscopic study of irradiation coloring of amazonite: structurally hydrous, Pb-bearing feldspar. Am Mineral 70:794-804

Hofmeister AM, Rossman GR (1986) A spectroscopic study of blue radiation coloring in plagioclase. Am Mineral 71:95-98
Hofmeister AM, Schaal RB, Campbell KR, Berry SL, Fagan TJ (1998) Prevalence and origin of birefringence in 48 garnets from the pyrope-almandine-grossularite-spessartine quaternary. Am Mineral 83:1293-1301
Ingrin J, Blanchard M (2006) Diffusion of hydrogen in minerals. Rev Mineral Geochem 62:291-320
Ingrin J, Skogby H (2000) Hydrogen in nominally anhydrous upper-mantle minerals: concentration levels and implications. Eur J Mineral 12:543-570
Ito Y, Nakashima S (2002) Water distribution in low-grade siliceous metamorphic rocks by micro-FTIR and its relation to grain size: A case from the Kanto Mountain region, Japan. Chem Geol 189:1-18
Johnson EA (2003) Hydrogen in nominally anhydrous crustal minerals. PhD Dissertation, California Institute of Technology, Pasadena, California
Johnson EA (2005) Magmatic water contents recorded by hydroxyl concentrations in plagioclase phenocrysts from Mount St. Helens, 1980-1981. Geochim Cosmochim Acta 69:A743
Johnson EA, Manning CE, Antignano A, Tropper P (2005) OH in rutile: an oxygen and water barometer. Eos Trans AGU 86(52), Fall Meet. Suppl.:Abstract V41A-1420
Johnson EA, Rossman GR (2003) The concentration and speciation of hydrogen in feldspars using FTIR and ^{1}H MAS NMR spectroscopy. Am Mineral 88:901-911
Johnson EA, Rossman GR (2004) A survey of hydrous species and concentrations in igneous feldspars. Am Mineral 89:586-600
Johnson EA, Rossman GR, Dyar MD, Valley JW (2002) Correlation between OH concentration and oxygen isotope diffusion rate in diopsides from the Adirondack Mountains, New York. Am Mineral 87:899-908
Johnson OW, DeFord J, Shaner JW (1973) Experimental technique for the precise determination of H and D concentration in rutile (TiO_2). J Appl Phys 44:3008-3012
Kalt A (2000) Cordierite channel volatiles as evidence for dehydration melting: an example from high-temperature metapelites of the Bayerische Wald (Variscan belt, Germany). Eur J Mineral 12:987-998
Kats A (1962) Hydrogen in alpha quartz. Phillips Research Report 17:133-279
Kekulawala KRSS, Paterson MS, Boland JN (1981) An experimental study of the role of water in quartz deformation. Geophysical Monograph 24:49-60
Keppler H, Bolfan-Casanova N (2006) Thermodynamics of water solubility and partitioning. Rev Mineral Geochem 62:193-230
Khomenko VM, Langer K (1999) Aliphatic hydrocarbons in structural channels of cordierite: a first evidence from polarized single-crystal IR-absorption spectroscopy. Am Mineral 84:1181-1185
King PL, Hervig RL, Holloway JR, Delaney JS, Dyar MD (2000) Partitioning of Fe^{3+}/Fe_{total} between amphibole and basanite melt as a function of oxygen fugacity. Earth Planet Sci Lett 178:97-112
Koch-Müller M, Dera P, Fei Y, Reno B, Sobolev N, Hauri E, Wysoczanski R (2003) OH- in synthetic and natural coesite. Am Mineral 88:1436-1445
Kohlstedt DL (2006) The role of water in high-temperature rock deformation. Rev Mineral Geochem 62: 377-396
Kolesov BA, Geiger CA (2000) Cordierite II: The role of CO_2 and H_2O. Am Mineral 85:1265-1274
Kronenberg (1994) Hydrogen speciation and chemical weakening of quartz. Rev Mineral 29:123-176
Kronenberg AK, Kirby SH, Aines RD, Rossman GR (1986) Solubility and diffusional uptake of hydrogen in quartz at high water pressures: Implications for hydrolytic weakening. J Geophys Res 91:12723-12744
Kronenberg AK, Wolf GH (1990) Fourier transform infrared spectroscopy determinations of intragranular water content in quartz-bearing rocks: implications for hydrolytic weakening in the laboratory and within the earth. Tectonophysics 172:255-271
Lager GA, Armbruster T, Faber J (1987a) Neutron and X-ray diffraction study of hydrogarnet $Ca_3Al_2(O_4H_4)_3$. Am Mineral 72:756-765
Lager GA, Armbruster T, Rotella FJ, Rossman GR (1989) OH substitution in garnets: X-ray and neutron diffraction, infrared, and geometric modeling studies. Am Mineral 74:840-851
Lager GA, Rossman GR, Rotella FJ, Schultz AJ (1987b) Neutron-diffraction structure of a low-water grossular at 20 K. Am Mineral 72:766-768
Lamb WM, Valley JW (1988) Granulite facies amphibole and biotite equilibria, and calculated peak-metamorphic water activities. Contrib Mineral Petrol 100:349-360
Lathe C, Koch-Müller M, Wirth R, van Westrenen W, Mueller H-J, Schilling F, Lauterjung J (2005) The influence of OH in coesite on the kinetics of the coesite-quartz phase transition. Am Mineral 90:36-43
Libowitzky E (1999) Correlation of O-H stretching frequencies and O-H···O hydrogen bond lengths in minerals. Mh Chemie 130:1047-1059
Libowitzky E, Beran A (2006) The structure of hydrous species in nominally anhydrous minerals: information from polarized IR spectroscopy. Rev Mineral Geochem 62:29-52
Locock A, Luth RW, Cavell RG, Smith DGW, Duke MJM (1995) Spectroscopy of the cation distribution in the schorlomite species of garnet. Am Mineral 80:27-38
Losos Z, Beran A (2004) OH defects in cassiterite. Mineral Petrol 81:219-234

Lumpkin GR (1998) Rare-element mineralogy and internal evolution of the Rutherford no.2 pegmatite, Amelia County, Virginia: A classic locality revisited. Can Mineral 36:339-353
Maldener J, Rauch F, Gavranic M, Beran A (2001) OH absorption coefficients of rutile and cassiterite deduced from nuclear reaction analysis and FTIR spectroscopy. Mineral Petrol 71:21-29
Maldener J, Hösch A, Langer K, Rauch F (2003) Hydrogen in some natural garnets studied by nuclear reaction analysis and vibrational spectroscopy. Phys Chem Minerals 30:337-344
McLennan SM, Taylor SR (1999) Earth's Continental Crust. *In:* Encyclopedia of Geochemistry. Marshall CP, Fairbridge RW (eds) Kluwer Academic Publishers, p 712
Miyoshi N, Yamaguchi Y, Makino K (2005) Successive zoning of Al and H in hydrothermal vein quartz. Am Mineral 90:310-315
Mosenfelder JL, Schertl HP, Smyth JR, Liou JG (2005) Factors in the preservation of coesite: The importance of fluid filtration. Am Mineral 90:779-789
Mottana A, Fusi A, Bianchi Potenza B, Crespi R, Liborio G (1983) Hydrocarbon-bearing cordierite from the Dervio-Colico road tunnel (Como, Italy). N Jb Mineral Abh 148:181-199
Nakano S, Makino K, Eriguchi T (2001) Microtexture and water content of alkali feldspar by Fourier-transform infrared microscopy. Mineral Mag 65:675-683
Nakashima S, Matayoshi H, Yuko T, Michibayashi K, Masuda T, Kuroki N, Yamagishi H, Ito Y, Nakamura A (1995) Infrared microspectroscopy analysis of water distribution in deformed and metamorphosed rocks. Tectonophysics 245:263-276
Nasdala L, Beran A, Libowitzky E, Wolf D (2001) The incorporation of hydroxyl groups and molecular water in natural zircon ($ZrSiO_4$). Am J Sci 301:831-857
Nash DB (1962) Contact metamorphism at Birch Creek, Blanco Mountain Quadrangle, Inyo County, California. MS Dissertation, University of California, Berkeley, California
Niimi N (2002) Static recrystallization of the deformed quartz in the granite from Mt. Takamiyama. J Geosci 45:89-100
O'Neil JR, Taylor Jr. HP (1967) The oxygen isotope and cation exchange chemistry of feldspars. Am Mineral 52:1414-1437
O'Neill B, Bass JD, Rossman GR (1993) Elastic properties of hydrogrossular garnet and implications for water in the upper mantle. J Geophys Res 98 (B11):20,031-20,037
Ord A, Hobbs BE (1986) Experimental control of the water-weakening effect in quartz. Geophysical Monograph 36:51-72
Peslier AH, Luhr J, Post JE (2002) Low water contents in pyroxenes from spinel-peridotites of the oxidized, sub-arc mantle wedge. Earth Planet Sci Lett 201:69-86
Post A, Tullis J (1998) The rate of water penetration in experimentally deformed quartzite: Implications for hydrolytic weakening. Tectonophysics 295:117-137
Rossman GR (1988) Vibrational spectroscopy of hydrous species. Rev Mineral 18:193-206
Rossman GR (1996) Studies of OH in nominally anhydrous minerals. Phys Chem Minerals 23:299-304
Rossman GR (2006) Analytical methods for measuring water in nominally anhydrous minerals. Rev Mineral Geochem 62:1-28
Rossman GR, Aines RD (1986) Spectroscopy of a birefringent grossular from Asbestos, Quebec, Canada. Am Mineral 71:779-780
Rossman GR, Aines RD (1991) The hydrous components in garnets: Grossular-hydrogrossular. Am Mineral 76: 1153-1164
Rossman GR, Rauch F, Livi R, Tombrello TA, Shi CR, Zhou ZY (1988) Nuclear reaction analysis of hydrogen in almandine, pyrope, and spessartite garnets. N Jb Mineral Mh 4:172-178
Rossman GR, Smyth JR (1990) Hydroxyl contents of accessory minerals in mantle eclogites and related rocks. Am Mineral 75:775-780
Rovetta MR, Holloway JD, Blacic JD (1986) Solubility of hydroxyl in natural quartz annealed in water at 900°C and 1.5GPa. Geophys Res Lett 13:145-148
Seaman SJ, Dyar MD, Marinkovic N, Dunbar NW (2006) An FTIR study of hydrogen in anorthoclase and associated melt inclusions. Am Mineral 91:12-20
Shieh YN, Taylor Jr. HP (1969) Oxygen and carbon isotope studies of contact metamorphism of carbonate rocks. J Petrol 10:307-331
Skogby H (2006) Water in natural mantle minerals I: pyroxenes. Rev Mineral Geochem 62:155-167
Skogby H, Bell DR, Rossman GR (1990) Hydroxide in pyroxene: variations in the natural environment. Am Mineral 75:764-774
Skogby H, Rossman GR (1989) OH^- in pyroxene; an experimental study of incorporation mechanisms and stability. Am Mineral 74:1059-1069
Smyth JR (2006) Hydrogen in high pressure silicate and oxide mineral structures. Rev Mineral Geochem 62: 85-115
Solomon GC, Rossman GR (1988) NH_4^+ in pegmatitic feldspars from the southern Black Hills, South Dakota. Am Mineral 73:818-821

Solomon GC, Taylor HP Jr (1991) Oxygen isotope studies of Jurassic fossil hydrothermal systems, Mojave Desert, southeastern California. *In:* Stable Isotope Geochemistry: A Tribute to Samuel Epstein. Taylor HP Jr, O'Neil JR, Kaplan IR (eds), The Geochemical Society, Special Publication Vol 3, p 449-462

Swamy V, Godhavari KS, Menon AG, Anantha Iyer GV (1992) Channel volatiles of south Indian cordierites as indicators of metamorphic fluid composition. N Jb Mineral Mh 8:359-375

Swope RJ, Smyth JR, Larson AC (1995) H in rutile-type compounds: I. Single-crystal neutron and X-ray diffraction study of H in rutile. Am Mineral 80:448-453

Tullis J, Yund RA (1980) Hydrolytic weakening of experimentally deformed Westerly granite and Hale albite rock. J Struct Geol 2:439-451

Van Baalen MR (1993) Titanium mobility in metamorphic systems: a review. Chem Geol 110:233-249

Vedder W, Wilkins RWT (1969) Dehydroxylation and rehydroxylation, oxidation and reduction of micas. Am Mineral 54:482-509

Visser D, Kloprogge JT, Maijer C (1994) An infrared spectroscopic (IR) and light element (Li, Ba, Na) study of cordierites from the Bamble Sector, South Norway. Lithos 32:95-107

Vlassopoulos D, Rossman GR, Haggerty SE (1993) Coupled substitution of H and minor elements in rutile and the implications of high OH contents in Nb- and Cr-rich rutile from the upper mantle. Am Mineral 78: 1181-1191

Vry JK, Brown PE, Valley JW (1990) Cordierite volatile content and the role of CO_2 in high-grade metamorphism. Am Mineral 75:71-88

Wilkins RWT, Sabine W (1973) Water content of some nominally anhydrous silicates. Am Mineral 58:508-516

Woodhead JA, Rossman GR, Thomas AP (1991a) Hydrous species in zircon. Am Mineral 76:1533-1546

Woodhead JA, Rossman GR, Silver LT (1991b) The metamictization of zircon: Radiation dose-dependent structural characteristics. Am Mineral 76:74-82

Xia Q, Pan Y, Chen D, Kohn S, Zhi X, Guo L, Cheng H, Wu Y (2000) Structural water in anorthoclase megacrysts from alkalic basalts: FTIR and NMR study. Acta Petrol Sinica 16:485-491

Yund RA (1983) Diffusion in feldspars. Rev Mineral 2:203-222

Yund RA, Ackermand D (1979) Development of perthite microstructures in the Storm King Granite, N.Y. Contrib Mineral Petrol 70:273-280

Yund RA, Anderson TF (1978) The effect of fluid pressure on oxygen isotope exchange between feldspar and water. Geochim Cosmochim Acta 42:235-239

Zhang M, Groat L, Salje EKH, Beran A (2001) Hydrous species in crystalline and metamict zircons. Am Mineral 86:904-909

APPENDIX

DATA TABLES OF HYDROUS SPECIES CONCENTRATIONS IN NOMINALLY ANHYDROUS CRUSTAL MINERALS

The following data tables summarize the quantitative measurements of hydrous species discussed or graphed in this chapter. Published works containing infrared spectra of quartz and cordierite are listed according to date; individual measurements are listed under each referenced work for feldspars, pyroxenes, garnets, kyanite, sillimanite, rutile, and cassiterite.

Studies of hydrogen in quartz.

Hydrolytic Weakening and Deformation Studies

Reference	Title
Griggs (1967)	Hydrolytic weakening of quartz and other silicates
Kekulawala et al. (1981)	An experimental study of the role of water in quartz deformation
Kronenberg et al. (1986)	Solubility and diffusional uptake of hydrogen in quartz at high water pressures: Implications for hydrolytic weakening
Rovetta et al. (1986)	Solubility of hydroxyl in natural quartz annealed in water at 900 °C and 1.5 GPa
Ord and Hobbs (1986)	Experimental control of the water-weakening effect in quartz
Cordier et al. (1988)	Water precipitation and diffusion in wet quartz and wet berlinite $AlPO_4$
Gerretsen et al. (1989)	The uptake and solubility of water in quartz at elevated pressure and temperature
Kronenberg and Wolf (1990)	Fourier transform infrared spectroscopy determinations of intragranular water content in quartz-bearing rocks: Implications for hydrolytic weakening in the laboratory and within the earth
Post and Tullis (1998)	The rate of water penetration in experimentally deformed quartzite: Implications for hydrolytic weakening

Geologic Surveys

Reference	Title
Berzina et al. (1991)	Water in quartz of Cu-Mo deposits
Nakashima et al. (1995)	Infrared microspectroscopy analysis of water distribution in deformed and metamorphosed rocks
Ito and Nakashima (2002)	Water distribution in low-grade siliceous metamorphic rocks by micro-FTIR and its relation to grain size: A case from the Kanto Mountain region, Japan
Niimi (2002)	Static recrystallization of the deformed quartz in the granite from Mt. Takamiyama

Geological studies of H_2O and CO_2 in cordierite.

Reference	Title
Armbruster et al. (1982)	Very high CO_2 cordierite from Norwegian Lapland: Mineralogy, petrology and carbon isotopes
Mottana et al. (1983)	Hydrocarbon-bearing cordierite from the Dervio-Colico road tunnel (Como, Italy)
Vry et al. (1990)	Cordierite volatile content and the role of CO_2 in high-grade metamorphism
Swamy et al. (1992)	Channel volatiles of south Indian cordierites as indicators of metamorphic fluid composition
Visser et al. (1994)	An infrared spectroscopic (IR) and light element (Li, Be, Na) study of cordierites from the Bamble Sector, South Norway
Kalt (2000)	Cordierite channel volatiles as evidence for dehydration melting: an example from high-temperature metapelites of the Bayerische Wald (Variscan belt, Germany)

Hydrous species in feldspars.

Sample Number	Feldspar composition/ structure	Occurrence	Species*	ppm H_2O wt.
	Data from Hofmeister (1985a)			
15020	amazonite; deep blue	pegmatite	H_2O	650
15020	amazonite; green	pegmatite	H_2O	900
15021	amazonite	pegmatite	H_2O	1100
	Data from Xia et al. (2000)			
NSC20	anorthoclase	alkali basalt	OH	405
PSSC3	anorthoclase	alkali basalt	OH, H_2O?	915
HNBC4	anorthoclase	alkali basalt	OH	365
	Data from Johnson and Rossman and references therein (2004)			
968	microcline	pegmatite	H_2O	1000
1281	microcline	pegmatite	H_2O	1350
1533	microcline	pegmatite	NH_4^+	542
2066	microcline	pegmatite	H_2O	135
			fi	196
CIT19237	microcline	pegmatite	fi	674
			NH_4^+	454
CIT19249	microcline	pegmatite	fi	878
146	orthoclase	pegmatite	OH	4
1275	orthoclase	pegmatite	OH	5
1618	orthoclase (adularia)	pegmatite	OH, H_2O	80
CIT10774	orthoclase	pegmatite	alteration	1949
			fi	1351
2063	sanidine	pegmatite	OH	1
680	albite	pegmatite	OH	192
901	albite	pegmatite	fi	248
			OH	
904	albite	pegmatite	OH	247
1605	albite	pegmatite	fi	39
			OH	
1608	albite	pegmatite	OH	
			fi	114
1609	albite	pegmatite	OH	
			fi	37
1610	albite	pegmatite	fi	13
2066	albite	pegmatite	fi	518
			OH	
580	oligoclase	pegmatite	OH	290
681	oligoclase	pegmatite	OH	21
HPT	anorthite	pegmatite	alteration	1401
			fi	574
1532	hyalophane	pegmatite	NH_4^+	1500
638	sanidine	volcanic	OH	170
JB1	sanidine	volcanic	OH	93
JV1	sanidine	volcanic	OH	14
1554	anorthoclase	volcanic	OH	238
1276a	anorthoclase	volcanic	OH	322
1277	anorthoclase	volcanic	OH	270
1280	oligoclase	volcanic	OH	230
1276b	andesine	volcanic	OH	249
1389	andesine	volcanic	OH	510
1604	andesine	volcanic	OH	4
15	labradorite	volcanic	OH	0
25	labradorite	volcanic	OH	125
145	labradorite	volcanic	nd	0
289	labradorite	volcanic	OH	18
1613	labradorite	volcanic	OH	21
1615	labradorite	volcanic	OH	4
1679	labradorite	volcanic	OH	80
1920	labradorite	volcanic	nd	0
1606	bytownite	volcanic	OH	46

Hydrous species in feldspars (continued)

Sample Number	Feldspar composition/ structure	Occurrence	Species*	ppm H_2O wt.
	Data from Johnson and Rossman and references therein (2004)			
1597	anorthite	volcanic	OH	180
1884	anorthite	volcanic	OH	115
1968	anorthite	volcanic	OH	210
M-1	anorthite	volcanic	mi	56
144	plagioclase	volcanic	OH	1
97KC02	plagioclase	volcanic	mi	46
URA5	plagioclase	volcanic	OH	25
ARG4b	feldspar	volcanic	mi	11
B45 HPT	alkali feldspar	plutonic	fi	700
			alteration	362
HPT	alkali feldspar	plutonic	fi	1299
			alteration	607
S-12 HPT	oligoclase	plutonic	inclusions	2092
CIT19224	andesine	plutonic	fi	1374
			alteration	1008
1550	andesine	plutonic	fi	287
			alteration	350
CIT19234	labradorite	plutonic	fi	65
			alteration	6
CIT19232	bytownite	plutonic	inclusions	77
CIT19230	anorthite	plutonic	fi	369
			alteration	338
CIT19231	plagioclase	plutonic	fi	322
			alteration	307
B46c HPT	plagioclase	plutonic	fi	1992
			alteration	3426
81-205 HPT	plagioclase	plutonic	alteration	1346
D81-75 HPT	plagioclase	plutonic	fi	831
			alteration	421
81-SR3	plagioclase	plutonic	nd	0
83-AUS-11	plagioclase	plutonic	nd	0
RT3#1	plagioclase	plutonic	inclusions	263
GCS026 (PUP11)	feldspar	plutonic	fi	382
PI 210 HPT	feldspar	plutonic	alteration	3900
Sky-9 HPT	feldspar	plutonic	fi	359
Plutonic Series: Fry Mountains Pluton				
GCS349	plagioclase	plutonic	fi	812
GCS348	plagioclase	plutonic	fi	1511
GCS284	orthoclase	plutonic	fi	2321
GCS283	plagioclase	plutonic	fi	1375
GCS280	plagioclase	plutonic	fi	4265
Plutonic Series: Skaergaard Intrusion				
KG-109 HPT	plagioclase	plutonic	OH	82
			alteration	121
SK-15 HPT	plagioclase	plutonic	fi	409
			alteration	3786
KG-236 HPT	plagioclase	plutonic	fi	1078
			alteration	666
Plutonic Series: Southern Idaho Batholith				
RH 68 HPT	feldspar	plutonic	fi	123
RB 163 HPT	alkali feldspar	plutonic	fi	2161
	Data from Seaman et al. (2006)			
Mt. Erebus	anorthoclase	volcanic	OH	126

*nd = not determined; fi = fluid inclusions; mi = melt inclusions

Structural hydroxyl concentrations in crustal and mantle pyroxenes.

Sample Number	Pyx. composition	Occurrence	wt% OH	[OH] ppm H_2O wt.*
		Data from Skogby et al. (1990)		
47	omphacite	eclogite xenolith in kimberlite	0.12	636
20	augite	xenolith in basalt	0.1	530
30	aegirine	authigenic	0.088	466
13	diopside	high-grade pyroxeneite	0.085	450
17	augite	xenocryst mantle diatreme	0.073	387
16	diopside	xenocryst mantle diatreme	0.073	387
7	diopside	megacryst in basalt	0.066	350
32	enstatite	metamorphic	0.066	350
48	enstatite	megacryst in kimberlite	0.05	265
33	enstatite	metamorphic	0.05	265
50	diopside	metamorphic?	0.045	238
40	diopside	xenolith in basalt	0.037	196
1	spodumene	granitic pegmatite	0.041	217
3	diopside	metamorphic	0.028	148
9	augite	volcanic	0.027	143
46	augite	volcanic?	0.026	138
6	diopside	metamorphic	0.025	132
37	enstatite	boninite lava	0.022	117
5	diopside	metamorphic	0.018	95
39	hedenbergite	metamorphic	0.018	95
18	enstatite	lower crustal	0.016	85
12	diopside	metamorphic	0.016	85
8	aegirine-augite	neph. sy. pegmatite	0.015	79
10	diopside	metamorphic	0.014	74
51	augite	gabroic xenolith, basalt	0.014	74
19	enstatite	basalt xenolith	0.012	64
28	diopside	rhyolitic pumice	0.011	58
2	diopside	metamorphic	0.009	48
38	enstatite	low-P metamorphic	0.008	42
21	diopside	oxidized alkali picrite	0.007	37
31	enstatite	megacryst	0.006	32
4	diopside	calcite vein	0.006	32
36	enstatite	megacryst, anorthosite	0.005	26
35	esseneite	buchite	0.004	21
41	diopside	metamorphic	0.004	21
14	diopside	metamorphic limestone	0.003	16
29	aegirine	nepheline syenite	0.002	11
25	aegirine	neph. sy. pegmatite	0.001	5
34	fassaite	meteorite	0	0
		Data from Bell et al. (1995)		
PMR-53	augite	megacryst, kimberlite		268
KBH-1	enstatite	megacryst, kimberlite		186
		Data from Johnson et al. (2002)		
95ADK1A	diopside	granulite-facies marble		138
95AK8f	diopside	granulite-facies marble		134
95AK24	diopside	granulite-facies marble		81
95AK6	diopside	granulite-facies marble		55
		Data from Peslier et al. (2002)		
SLP-402	orthopyroxene	mantle wedge xenolith		189
SLP-402	clinopyroxene	mantle wedge xenolith		413
SLP-400	orthopyroxene	mantle wedge xenolith		140
SLP-403	orthopyroxene	mantle wedge xenolith		243
SLP-403	clinopyroxene	mantle wedge xenolith		528
SLP-101	orthopyroxene	mantle wedge xenolith		155
SLP-101	clinopyroxene	mantle wedge xenolith		398
SLP-114	orthopyroxene	mantle wedge xenolith		107
SLP-114	clinopyroxene	mantle wedge xenolith		222
SLP-405	orthopyroxene	mantle wedge xenolith		171
SLP-405	clinopyroxene	mantle wedge xenolith		373
SLP-142	orthopyroxene	mantle wedge xenolith		280

Structural hydroxyl concentrations in crustal and mantal pyroxenes (continued).

Sample Number	Pyx. composition	Occurrence	wt% OH	[OH] ppm H_2O wt.*
		Data from Peslier et al. (2002)		
SLP-142	clinopyroxene	mantle wedge xenolith		514
DGO-166	orthopyroxene	mantle wedge xenolith		166
DGO-166	clinopyroxene	mantle wedge xenolith		387
DGO-160	orthopyroxene	mantle wedge xenolith		86
DGO-160	clinopyroxene	mantle wedge xenolith		256
SIN-3	clinopyroxene	mantle wedge xenolith		288
BCN-200D	orthopyroxene	mantle wedge xenolith		190
BCN-200D	clinopyroxene	mantle wedge xenolith		477
BCN-130	orthopyroxene	mantle wedge xenolith		128
BCN-130	clinopyroxene	mantle wedge xenolith		313
BCN-201B	orthopyroxene	mantle wedge xenolith		203
BCN-201B	clinopyroxene	mantle wedge xenolith		342
BCN-203	orthopyroxene	mantle wedge xenolith		39
SIM-9c	orthopyroxene	mantle wedge xenolith		71
SIM-9c	clinopyroxene	mantle wedge xenolith		205
SIM-24	orthopyroxene	mantle wedge xenolith		115
SIM-24	clinopyroxene	mantle wedge xenolith		158
SIM-3	orthopyroxene	mantle wedge xenolith		109
SIM-3	clinopyroxene	mantle wedge xenolith		140
		Data from Filip et al. (2006)		
Sp14	spodumene	granitic pegmatite		1.4
Sp16	spodumene	granitic pegmatite		0.89
Sp26	spodumene	granitic pegmatite		0.82
SpKor	spodumene	granitic pegmatite		1.73
Sp01	spodumene	granitic pegmatite		3.78
Sp03	spodumene	granitic pegmatite		3.43
Sp04	spodumene	granitic pegmatite		1.21
Sp05	spodumene	granitic pegmatite		0.44
Sp06	spodumene	granitic pegmatite		1.09
Sp12	spodumene	granitic pegmatite		0.61
Sp13	spodumene	granitic pegmatite		2.49
Sp17	spodumene	granitic pegmatite		0.63
Sp25	spodumene	granitic pegmatite		1.81
Sp15	spodumene	granitic pegmatite		0.35
Sp20	spodumene	granitic pegmatite		0.41
Sp21	spodumene	granitic pegmatite		0.42
Sp22	spodumene	granitic pegmatite		0.72
Sp23	spodumene	granitic pegmatite		1.26
Sp02	spodumene	granitic pegmatite		0.53
Sp11	spodumene	granitic pegmatite		0.57
Sp18	spodumene	granitic pegmatite		0.64
Sp28	spodumene	granitic pegmatite		0.49
Sp07	spodumene	granitic pegmatite		0.4
Sp08	spodumene	granitic pegmatite		0.32
Sp10	spodumene	granitic pegmatite		0.24
Sp19	spodumene	granitic pegmatite		0.25
Sp24	spodumene	granitic pegmatite		0.39
Sp27a	spodumene	granitic pegmatite		0.21
Sp27b	spodumene	granitic pegmatite		0.29
Sp29	spodumene	granitic pegmatite		0.37
SpPak	spodumene	granitic pegmatite		0.13

* [OH] calculated using Bell et al. (1995) calibrations, except for samples from Skogby et al. (1990), which use calibration from that study (same within error of Bell et al. (1995) calibration), and Filip et al. (2006), which use the calibration from Libowitzky and Rossman (1997).
†Maximum reported concentration for each sample.

Structural hydroxyl concentrations in crustal garnets.

Sample Number	Garnet composition	Occurrence	wt% H_2O
	Data from Aines and Rossman (1984b)		
2	Spessartine	Pegmatite	0.084
4	Spessartine	Pegmatite	0.25
5	Almandine-Spessartine	Pegmatite	0.36
10	Spessartine-Almandine	?	0.059
12	Spessartine-Almandine	Pegmatite?	0.17
13	Grossular	Altered ultramafic body	0.18
35	Almandine-Pyrope	Gneiss	0.06
49	Pyrope	Diatreme megacryst	0.08
104	Almandine-Spessartine	Pegmatite	0.27
113	Pyrope	Diatreme	0.15
114	Pyrope	Diatreme	0.22
	Data from Rossman and Aines (1991)		
42	Grossular	Skarn	0.1
1359	Grossular	Metarodingite	0.28
1360	Grossular	Metarodingite	0.85
1409	Grossular	Skarn	0.185
1411	Grossular	Skarn	0.08
	Data from Locock et al. (1995)		
Ice River	Schorlomite	Alkaline complex	0.036
	Data from Amthauer and Rossman (1998)		
GRR1669	Hydroandradite	Basalt vug	5.92
GA33	Andradite	Serpentinite	0.01
GA34	Andradite	Serpentinite	0.07
GRR48 rim	Andradite	Serpentinite	0.1
GRR134	Andradite	Serpentinite	0.09
GRR169	Andradite	Serpentinite	0.15
GRR684	Melanite	Serpentinite	1.17
GRR1263	Melanite	Serpentinite	0.04
GRR1328	Melanite	Serpentinite	2.45
GRR1765	Demantoid	Serpentinite	0.1
GA32	Andradite	Skarn	0.15
GA35	Andradite	Skarn	0.05
GRR54	Andradite	Skarn	0.38
GRR149	Andradite	Skarn	0.04
GRR1015	Andradite	Skarn	1.44
GRR1137a2	Andradite	Skarn	0.4
GRR1447	Andradite	Skarn	0.03
GRR1448	Andradite	Skarn	0.01
GA24	Melanite	Phonolite	0.01
GA36	Melanite	Magmatic	0.03
GRR1446	Melanite	Magmatic	0.04
CITH3110	Melanite	Magmatic	0.02
	Data from Arredondo et al. (2001)		
Ru. 1	Spessartine	Pegmatite	0.023
Ru. 2	Spessartine	Pegmatite	0.022
Ru. 3	Spessartine	Pegmatite	0.083
Ru. 4	Spessartine	Pegmatite	0.127
Ru. 5	Spessartine	Pegmatite	0.128
Ru. 6	Spessartine	Pegmatite	0.134
Ru. 7	Spessartine	Pegmatite	0.13
Ru. 8	Spessartine	Pegmatite	0.158
Ru. 9	Spessartine	Pegmatite	0.147
Ru. 10	Spessartine	Pegmatite	0.121
Him. 1	Spessartine	Pegmatite	0.007
Him. 2	Spessartine	Pegmatite	0.009
Him. 3	Spessartine	Pegmatite	0.019
Him. 4	Spessartine	Pegmatite	0.034
GAB 0	Spessartine	Pegmatite	0.0026
GAB 30	Spessartine	Pegmatite	0.0034
GAB 60	Spessartine	Pegmatite	0.004

Structural hydroxyl concentrations in crustal garnets (continued).

Sample Number	Garnet composition	Occurrence	wt% H_2O
	Data from Arredondo et al. (2001)		
GAB 90	Spessartine	Pegmatite	0.006
GAB 120	Spessartine	Pegmatite	0.001
GAB 150	Spessartine	Pegmatite	0.0025
GAB 180	Spessartine	Pegmatite	0.0031
GAB 240	Spessartine	Pegmatite	0.0047
GAB 300	Spessartine	Pegmatite	0.0042
GAB 330	Spessartine	Pegmatite	0.0055
GAB 420	Spessartine	Pegmatite	0.0035
GAB 480	Spessartine	Pegmatite	0.0009
GAB 540	Spessartine	Pegmatite	0.0004
GAB 600	Spessartine	Pegmatite	0.0077
GAB 660	Spessartine	Pegmatite	0.0025
GAB 720	Spessartine	Pegmatite	0.0015
GAB 780	Spessartine	Pegmatite	0.0035
GAB 810	Spessartine	Pegmatite	0.0073
	Data from Johnson (2003)		
BC2B1	Grossular-andradite	Skarn	0.331
BC2B3	Grossular-andradite	Skarn	0.311
BC2B4	Grossular-andradite	Skarn	0.311
BC-11	Grossular-andradite	Skarn	0.182
W77-102	Grossular-andradite	Skarn	0.0592
99W-2	Grossular-andradite	Skarn	0.1862
99W-2	Grossular-andradite	Skarn	0.1842
W50-419	Grossular-andradite	Skarn	0.0277
99W-1	Grossular-andradite	Skarn	0.0466
99W-4	Grossular-andradite	Skarn	0.0342
99W-4	Grossular-andradite	Skarn	0.0211
W81-15 148′2″	Grossular-andradite	Skarn	0.0239
W81-15 148′2″	Grossular-andradite	Skarn	0.0282
W81-15 149′9″	Grossular-andradite	Skarn	0.0281
W81-15 149′9″	Grossular-andradite	Skarn	0.0247
W81-15 150′9″	Grossular-andradite	Skarn	0.0238
W81-15 150′9″	Grossular-andradite	Skarn	0.0171
W81-15 150′9″	Grossular-andradite	Skarn	0.0268
W81-15 321′	Grossular-andradite	Skarn	0.0524
W81-15 321′	Grossular-andradite	Skarn	0.0487
W81-15 321′	Grossular-andradite	Skarn	0.0363
W81-15 269′4″	Grossular-andradite	Skarn	0.0097
W81-15 269′10″	Grossular-andradite	Skarn	0.0161
W81-15 269′10″	Grossular-andradite	Skarn	0.0164
W81-15 270′5″	Grossular-andradite	Skarn	0.0494
W81-15 273′	Grossular-andradite	Skarn	0.0489
W81-15 276′2″	Grossular-andradite	Skarn	0.1264
W81-15 276′2″	Grossular-andradite	Skarn	0.1619
W81-15 276′5″	Grossular-andradite	Skarn	0.1117
W81-15 278′5″	Grossular-andradite	Skarn	0.0893
W81-15 282′5″	Grossular-andradite	Skarn	0.0865
W81-15 282′5″	Grossular-andradite	Skarn	0.0839
W81-15 285′	Grossular-andradite	Skarn	0.0177
W81-15 285′	Grossular-andradite	Skarn	0.0255
W81-15 299′6″	Grossular-andradite	Skarn	0.0922
W81-15 299′6″	Grossular-andradite	Skarn	0.1037
W81-15 301′8″	Grossular-andradite	Skarn	0.0751
W81-15 301′8″	Grossular-andradite	Skarn	0.0801
W81-15 304′	Grossular-andradite	Skarn	0.1453
W81-15 304′	Grossular-andradite	Skarn	0.1163
W81-15 307′	Grossular-andradite	Skarn	0.1165
W81-15 311′	Grossular-andradite	Skarn	0.0271
W81-15 313′6″	Grossular-andradite	Skarn	0.0333
W81-15 313′6″	Grossular-andradite	Skarn	0.0336
W81-15 313′6″	Grossular-andradite	Skarn	0.0304
W81-15 314′	Grossular-andradite	Skarn	0.0033
W81-15 314′	Grossular-andradite	Skarn	0.0040
W81-15 318′7″	Grossular-andradite	Skarn	0.0381
W81-15 318′7″	Grossular-andradite	Skarn	0.0417

Structural hydroxyl concentrations in crustal garnets (continued).

Sample Number	Garnet composition	Occurrence	wt% H_2O
	Data from Johnson (2003)		
W81-15 328′6″	Grossular-andradite	Skarn	0.0039
W81-15 347′7″	Almandine	Anorthosite	0.0000
W81-15 347′7″	Almandine	Anorthosite	0.0000
W81-15 370′	Almandine	Anorthosite	0.0039
W81-15 396′8″	Grossular-andradite	Skarn	0.0294
W81-15 396′8″	Grossular-andradite	Skarn	0.0410
W81-15 404′3″	Grossular-andradite	Skarn	0.1333
W81-15 404′3″	Grossular-andradite	Skarn	0.1353
W81-15 407′2″	Grossular-andradite	Skarn	0.1653
W81-15 407′2″	Grossular-andradite	Skarn	0.1659
W81-15 411′	Grossular-andradite	Skarn	0.0383
W81-15 411′	Grossular-andradite	Skarn	0.0597
W81-15 33_′0″	Grossular-andradite	Skarn	0.0474
W81-15 33_′0″	Grossular-andradite	Skarn	0.0712
103′3″	Grossular-andradite	Skarn	0.0485
103′3″	Grossular-andradite	Skarn	0.0703
113′6″	Grossular-andradite	Skarn	0.0159
113′6″	Grossular-andradite	Skarn	0.0180
134′4″	Grossular-andradite	Skarn	0.0669
136′8″ And.	Grossular-andradite	Skarn	0.0778
136′8″ Gros.	Grossular-andradite	Skarn	0.0619
136′8″ Gros.	Grossular-andradite	Skarn	0.0814
138′10″	Grossular-andradite	Skarn	0.0751
139′9″ gt	Grossular-andradite	Skarn	0.0798
139′9″ gt	Grossular-andradite	Skarn	0.0877
139′9″	Grossular-andradite	Skarn	0.0707
139′9″	Grossular-andradite	Skarn	0.0780
140′7″	Grossular-andradite	Skarn	0.0439
140′7″	Grossular-andradite	Skarn	0.0720
140′7″	Grossular-andradite	Skarn	0.0783
144′2″	Grossular-andradite	Skarn	0.1402
144′2″	Grossular-andradite	Skarn	0.1480
144′6″ And.	Grossular-andradite	Skarn	0.1175
148′3″	Grossular-andradite	Skarn	0.1081
148′3″	Grossular-andradite	Skarn	0.1075
154′5″	Grossular-andradite	Skarn	0.0070
154′5″	Grossular-andradite	Skarn	0.0112
154′5″	Grossular-andradite	Skarn	0.0108
158′2″	Grossular-andradite	Skarn	0.0118
158′5″	Grossular-andradite	Skarn	0.0236
162′6″	Grossular-andradite	Skarn	0.0466
162′6″	Grossular-andradite	Skarn	0.0822
167′8″	Grossular-andradite	Skarn	0.0293
167′8″	Grossular-andradite	Skarn	0.0285
171′6″	Grossular-andradite	Skarn	0.0725
174′9″	Grossular-andradite	Skarn	0.0751
174′9″	Grossular-andradite	Skarn	0.0795
177′	Grossular-andradite	Skarn	0.0155
177′	Grossular-andradite	Skarn	0.0142
190′	Grossular-andradite	Skarn	0.0565
194′6″	Grossular-andradite	Skarn	0.0323
194′6″	Grossular-andradite	Skarn	0.0349
200′3″	Grossular-andradite	Skarn	0.0524
205′9″	Grossular-andradite	Skarn	0.0829
206′2″	Grossular-andradite	Skarn	0.1016
210′6″	Grossular-andradite	Skarn	0.0832
215′8″	Grossular-andradite	Skarn	0.1087
218′8″	Grossular-andradite	Skarn	0.0912
219′8″	Grossular-andradite	Skarn	0.1077
219′8″	Grossular-andradite	Skarn	0.0970
221′	Grossular-andradite	Skarn	0.0789
226′	Grossular-andradite	Skarn	0.0857
226′	Grossular-andradite	Skarn	0.1163
238′3″	Grossular-andradite	Skarn	0.1451
238′3″	Grossular-andradite	Skarn	0.1385

Structural hydroxyl concentrations in crustal garnets (continued).

Sample Number	Garnet composition	Occurrence	wt% H_2O
	Data from Johnson (2003)		
238′8″	Grossular-andradite	Skarn	0.1185
239′10″	Grossular-andradite	Skarn	0.0221
239′10″	Grossular-andradite	Skarn	0.0354
245′6″	Grossular-andradite	Skarn	0.1210
245′6″	Grossular-andradite	Skarn	0.1217
247′10″	Grossular-andradite	Skarn	0.0950
247′10″	Grossular-andradite	Skarn	0.1144
248′2″	Grossular-andradite	Skarn	0.0505
248′2″	Grossular-andradite	Skarn	0.1111
248′2″	Grossular-andradite	Skarn	0.1143
251′	Grossular-andradite	Skarn	0.0610
253′	Grossular-andradite	Skarn	0.0692
254′6″	Grossular-andradite	Skarn	0.1014
254′6″	Grossular-andradite	Skarn	0.1121
259′8″	Grossular-andradite	Skarn	0.1021
259′11″	Grossular-andradite	Skarn	0.1105
259′11″	Grossular-andradite	Skarn	0.1221
261′1″	Grossular-andradite	Skarn	0.0914
261′1″	Grossular-andradite	Skarn	0.1131
267′	Grossular-andradite	Skarn	0.0626
267′	Grossular-andradite	Skarn	0.1088
271′9″	Grossular-andradite	Skarn	0.1483
271′9″	Grossular-andradite	Skarn	0.1490
278′6″	Grossular-andradite	Skarn	0.0806
278′6″	Grossular-andradite	Skarn	0.0977
282′3″	Grossular-andradite	Skarn	0.0874
282′3″	Grossular-andradite	Skarn	0.0909
283′4″	Grossular-andradite	Skarn	0.0845
285′6″	Grossular-andradite	Skarn	0.0787
285′6″	Grossular-andradite	Skarn	0.1022
287′2″	Grossular-andradite	Skarn	0.0393
289′3″	Grossular-andradite	Skarn	0.0250
289′3″	Grossular-andradite	Skarn	0.0460
	Data from Maldener et al. (2003)		
RHOTAN1	Pyrope-almandine		0.0019
PYALTAN	Pyrope-almandine		0.0017
RHOTAN2	Pyrope-almandine		0.0018
HAI	Almandine-pyrope		0.0018
RAJA	Almandine-pyrope		0.0014
GTALX	Almandine-pyrope		0.0048
SPESSOR	Spessartine		0.0025
HESSI(thick)	Grossular		0.0950
HESSI(thin)	Grossular		0.0870
TSAV	Grossular		0.0480
MALI	Grossular-andradite		0.0170
GRMALI	Grossular-andradite		0.0190

Structural hydroxyl concentrations in kyanite.

Sample Number	Rock Type	*P* (kbar)	*T* (°C)	[OH] ppm H_2O wt%	[OH] (ppm H_2O wt%) using Bell et al. (2004)
	Data from Beran and Götzinger (1987) and references within				
1	Granulite	5-10	530-710	50	3
2	Granulite	5-10	530-710	50	3
3	Gt-ky-st-mica schist	?	?	50	3
4	Cor-fuchsite-ky greenstone belt	5-7	550-650	100	6
5	Eclogite	?	?	450	25
6	Eclogite	6-10	330-550	500	28
7	Eclogite	5.5-9	500-660	750	42
8	Eclogite	6-10	330-550	800	44
9	Gneiss (ky-st-qtz-fsp)	4-8	500-600	800	44
10	Eclogite	28-32	750-850	1800	100
	Data from Beran et al. (1993)				
G1/Ky3	Eclogite			410	23
	Data from Bell et al. (2004a)				
H105650	Eclogite				4
H85943	Eclogite?				22
LTL-3	Eclogite				27
FSM-15	Eclogite				230

Structural hydroxyl concentrations in sillimanite.

Sample Number	Rock Type*	Total OH band absorbance (cm^{-1})	Est. [OH] ppm H_2O wt%†
	Data from Beran et al. (1989)		
GRR273	HG	0.408	44
GRR439	HG	0.472	51
GRR385	X	0.096	10
GRR380	HG	0.547	59
GRR1585	UA	0.056	6
GRR384	UA	0	0
GRR547	UA	0.744	81
GRR383	UA	0.452	49
GRR450	UA	0.791	86
GRR382	?	1.263	137
GRR608	PG	0.193	21
GRR386	UA	0.908	98
GRR311	X	0	0
GRR509	AG	1.14	123
GRR306	X	0.351	38
GRR560	PG	0	0
GRR1485	AG	0.085	9
AB-Gho	UA	1.129	122
AB-Sm1	AG	1.848	200
GRR799	HG	0.924	100
GRR802	PG	0	0

* AG = alluvial deposit, presumably from granulite facies; HG = hornblende granulite facies; PG = pyroxene granulite facies; UA = upper amphibolite grade; X = xenolithic.
† OH concentration estimated from thermal weight loss data in Beran et al. (1989).

Structural hydroxyl concentration in andalusite.

Sample Number	Locality	[OH] ppm H_2O wt%*
	Data from Rossman (1996)	
GRR273	Minas Gerais, Brazil	270

Structural hydroxyl concentrations in rutile.

Sample Number	Rock Type	[OH] ppm H_2O wt%*	[OH] (ppm H_2O wt%) using Maldener et al. (2001)
	Data from Rossman and Smyth (1990)		
EJ-86b	eclogite	240	2257
	Data from Hammer and Beran (1991)		
1	pegmatite	900	310
2	pegmatite	1300	447
3	pegmatite	1000	344
4	unknown	900	310
5	pegmatite	900	310
6	pegmatite	1600	551
7	pegmatite	900	310
8	xenolith?	1600	551
9	phyllite	1000	344
10	amphibolite	1800	620
11	mica schist	1800	620
12	amphibolite	1400	482
13	chl-mica schist	1500	516
14	chl-mica schist	1100	379
15	amphibolite	1900	654
16	amphibolite	2100	723
17	amphibolite	1600	551
18	eclogite	800	275
19	blueschist (pyrope incl.)	400	138
	Data from Vlassopoulos et al. (1993)		
R-1	Ky+rut+lazulite	2900	1001
R-2	Ky+rut+lazulite	3100	1074
R-4	carbonatite	1200	416
R-5	unknown	1000	333
R-6	mt+ap+chl schist	2800	962
R-7	hydrothermal vein	1200	401
R-8	hydrothermal vein	4800	1666
JAG83-30-1	rt-ilm xenolith	5400	1887
JAG83-30-2	rt-ilm xenolith	6000	2084
JAG83-30-3	rt-ilm xenolith	8000	2768
JAG85-2	rt-ilm xenolith	2500	868
	Data from Maldener et al. (2001)		
R5	pegmatite		70
R5a	pegmatite		330
R6	pegmatite		820
R7a	pegmatite		270

* Determined using the integrated absorption coefficient from Hammer and Beran (1991).

Structural hydroxyl concentrations in cassiterite.

Sample Number	Locality	[OH] ppm H_2O wt%
	Data from Maldener et al. (2001)	
CC	Cornwall	170
ZZ	Zinnwald	160
	Data from Losos and Beran (2004)	
4	Greisen	49
6	Greisen	110
10	Greisen	93
11	Hydrothermal vein	120
12	?	32
13	Cassiterite-sulphide deposit	170
14	Tin melt (synthetic)	2
15	Tin melt (synthetic)	8
16	Greisen/quartz vein	90
17	?	32
18	Cut gemstone	82